CHARACTERISTICS OF TIDALLY-FORCED POLLUTANT TRANSPORT IN NARROW CHANNELS

by

Michael J. B. Cole

B.Sc.E., Queen's University, Kingston, 1989

A THESIS SUBMITTED IN PARTIAL FULFILMENT OF

THE REQUIREMENTS FOR THE DEGREE OF

MASTER OF APPLIED SCIENCE

in

THE FACULTY OF GRADUATE STUDIES

Department of Civil Engineering

We accept this thesis as conforming

to the required standard

THE UNIVERSITY OF BRITISH COLUMBIA

September 1992

In presenting this thesis in partial fulfilment of the requirements for an advanced degree at the University of British Columbia, I agree that the Library shall make it freely available for reference and study. I further agree that permission for extensive copying of this thesis for scholarly purposes may be granted by the head of my department or by his or her representatives. It is understood that copying or publication of this thesis for financial gain shall not be allowed without my written permission.

(Signature)

Department of Civil Engineering

The University of British Columbia
Vancouver, Canada

Date Oct 5th '92

Abstract

Physical and numerical model studies have been conducted to lend insight to the subject of transport and dispersion of a neutrally buoyant effluent released instantaneously from a point source into a one-dimensional tidal body. Closed-form expressions are obtained for the fluid velocity and free surface elevation due to tidal forcing in a one-dimensional channel. Physical experiments were conducted in the Hydraulics Laboratory of the Department of Civil Engineering at the University of British Columbia, and measurements of both effluent concentration and velocity along the test channel were recorded. A numerical model based on the Finite Difference Method was developed for computing the time-varying effluent concentration within the channel. The influence of grid size and time step used in the numerical model was examined. The following parameters were varied: effluent discharge location, release time within the tidal cycle, average water depth, tidal amplitude, and tidal period. The experimental measurements and numerical predictions were correlated to derive an effective one-dimensional diffusion coefficient for the numerical model. The numerical results suggest that the fluid velocity at the instant and location of pollutant release is of primary importance to the mixing of the pollutant cloud into the surrounding waters.

Table Of Contents

List of Tables

List of Figures

Abbreviations

A	=	tidal amplitude (m)
A_r	=	cross-sectional area in the y and z directions (m^2)
c	=	shallow wave celerity (m/s)
Co	=	initial concentration (mg/l or parts per thousand)
C	=	pollutant concentration (mg/l or parts per thousand)
C_r	=	Courant number
d	=	average water depth (m)
D	=	diffusion coefficient (m^2/s)
g	=	gravitational constant (m/s^2)
H	=	total water depth (m) equal to $d + \eta$
k	=	$2\pi/L$ (m^{-1})
K	=	roughness parameter
K_d	=	decay coefficient
M	=	Mass of pollutant (kg)
P_e	=	Peclet number
q	=	source/sink term
Re	=	Reynolds number
t	=	time (s)
t_o	=	initial discharge time (s)
T	=	tidal period (s)
T_e	=	duration of effluent outflow (s)
U	=	velocity in the x-direction (m/s)
V	=	velocity in the y-direction (m/s)
W	=	velocity in the z-direction (m/s)
x	=	position along channel direction (m)
x_c	=	position of pollutant concentration measurement (m)
x_p	=	position of pollutant discharge (m)
y	=	position in the cross channel direction (m)
z	=	position in the vertical direction (m)
γ	=	ratio of advection to diffusion
η	=	water elevation relative to the still water level (m)
λ	=	length of channel in the x-direction (m)
ρ	=	fluid density (kg/m^3)
ω	=	$2\pi/T$ (rad/s)
υ	=	kinematic viscosity (m^2/s)
δ	=	Dirac function

Acknowledgment

The author would like to express his profound gratitude to his supervisor Dr. M. Isaacson for his help and encouragement throughout this project. Thanks are also extended to Dr. G. Lawrence who assisted in the supervision of this thesis and offered valuable insight into its subject.

The author would also like to acknowledge his friends and colleagues in the Coastal Engineering group at UBC without whom this thesis would not have materialized. The never-ending assistance of S. Prasad and N. Yonemitsu is especially appreciated. Technical support from Kurt, and Ron of the Civil Engineering technical staff is also gratefully noted.

Finally, the author wishes to thank Benjamin B. for providing a most conducive atmosphere in which to write the majority of this thesis.

Chapter 1 - Introduction

1.1 General

The characteristics of pollutant transport within channels and harbours are of interest for various reasons. With increasing urbanization and use of recreational watercraft along the British Columbia coast, the amount of pollutants entering our coastal waters is expected to increase. Coincident with this increase is an ever-growing concern for the environment and our water quality. These concerns affect decisions relating to the design and placement of man-made coastal features such as harbours and outflow pipes and influence the extent and manner in which effluents are discharged.

Local pollutants that enter enclosed waters as a direct result of boating activities include anti-fouling paint, fuel spills, and runoff from various related works (such as loading docks and shipyards). In addition, non-related pollutant sources include industrial effluent discharged from tributaries, sewage and storm water outfalls. These pollutants affect a channel's water quality and ultimately affect the water quality outside the channel. The extent of any environmental consequences related to a specific pollutant release depend on:

1) toxicity,
2) initial pollutant concentrations,
3) the rate at which the pollutant is mixed into the surrounding waters, and
4) the subsequent rate of decay or rate of expulsion (or flushing) of these affected waters from the local zone.

The rate of mixing depends on various hydrodynamic factors (including circulation) of the channel and on the diffusion characteristics of the pollutant. One would expect that the faster the

mixing and flushing occur, the less severe the immediate environmental effects (being related to lower overall pollutant concentrations within the channel).

Generalized Case

In the general case, some of the more significant factors affecting pollutant transport include the following:

Pollutant Outflow	- point source (continuous or instantaneous) - line source (continuous or instantaneous) - multiple sources at various locations within a basin or channel - stage of a tidal cycle at which pollutants are released
Stratification	- estuarine conditions of prominent fresh and salt water layers - variations in density between the pollutant and the surrounding water
Tidal Range	- variations of the tidal range to average depth ratio
Return Flow	- variations in the tidal prism describing the return of pollutant to the channel on the flood tide
Hydraulic Forcing	- river and groundwater sources causing mixing and/or stratification
Channel Geometries	- broad or narrow entrance conditions - length to breadth variations - length to depth variations
External Mixing	- wind forcing - wave action
Hydrodynamics	- linear and nonlinear considerations
Friction Effects	- variations in flow and turbulence
Flow Constraints	- retarding effects of irregular channels and mooring structures

The tidal prism mentioned above, is defined as the percentage of harbour water that exitted on the ebb tide and returns from the sea during a flood tide. This percentage is dependent on the effects of logshore drift.

Local Concerns

The significant tidal range in British Columbia suggests the occurrence of large flushing and transport rates in coastal channels and harbours. In channels such as False Creek, Vancouver, where there are complex pier interactions and the channel shape is long and narrow, one would expect flushing rates to be low and mixing rates to be unpredictable. Because of the rocky coastline in British Columbia, groundwater intrusion is usually not a concern. Local winds along the coast are irregular and seasonally dependent. Phenomena such as outflow winds can create extremely strong surface shears for extended periods during winter months. Furthermore, since the summer months are the period of greatest channel activity (due to pleasure craft), flushing and transport mechanisms dominant during this period are of the greatest importance for any boat related pollutants.

Potential Benefits of Research

If the transport characteristics of a pollutant are known, monitoring programs can be conducted more efficiently, by testing at locations thought to be most affected. In the case of pollutants that need to be traced at levels close to their detection limits, time and money can be saved by omitting dilute areas from monitoring programs. Remediation and worst-case scenarios can be forecast to aid in possible clean-up operations.

1.2 Assumptions and Direction of Research

The term 'pollutant transport' is used to denote the movement of pollutant due to advective and diffusive processes. The advective processes move both the pollutant and the surrounding fluid along the channel without diluting the pollutant or distorting it's shape. The fluid's movement is

governed by hydrodynamic processes relating to the effects of viscosity, density, and gravity.

The diffusive processes at work within this system are comprised of two main components:

1) shear flow dispersion
2) turbulent diffusion

Shear flow dispersion is, itself, a function of the hydrodynamic conditions within the channel. Vertical velocity variations cause shearing of the fluid and molecular diffusion occurs over this interface. Turbulent diffusion is a function of the channel velocity and of the turbulent mixing length which decribes the magnitude of the turbulent processes at hand. The major source of mixing within the experiment is due to shear dispersion which is typically the major source of diffusion in estuaries (Fischer et al., 1979).

Pollutant transport in an inlet can be characterized as one, two, or three dimensional on the basis of the importance of depth-wise and width-wise variations of flow velocities and resulting pollutant transport. A one-dimensional (denoted 1-D) situation corresponds to no significant depth or width variations and corresponding low velocities in these directions.

In this context, Figure 1.1 shows three separate shallow water channel configurations denoted 1-D, 1.5-D, and 2-D. These three situations are based on the assumption that the channel depth is relatively shallow so that mixing occurs quickly in the vertical and velocities in the vertical direction are negligible.

In the first case (1-D) , it is assumed that mixing and transport of a pollutant is dominated by one-dimensional constant width flow, with velocities and mixing occurring primarily in the horizontal plane only (simulating shallow water conditions) and only along the axis of the inlet. A 1.5-D channel is essentially an extension to the 1-D case such that the channel width may vary but it is assumed that the flow in the cross-channel direction, y, is negligible. The 2-D case assumes both flow and transport in both the x and y directions to be significant.

Within the context of this thesis, research has been conducted on one-dimensional situations. More specifically and particularly applicable to the British Columbia coast, this corresponds to the study of transport in long narrow inlets.

Domain of Study Case

Of the influencing factors listed in Section 1.1, a few have been selected and studied in this thesis. For the one-dimensional case the instantaneous release of pollutant for various channel geometries and at various stages of the tidal cycle have been studied. In particular, the characteristics studied within this thesis include,

1) 1-D channel
2) instantaneous point-source release of pollutant
3) a neutrally buoyant pollutant
4) no return flow of pollutant
5) no hydraulic forcing from additional inlets to the channel

To simplify the situation, return flow of pollutant on the tides was neglected. Also, the effects of river inflow are not studied. These do not, however, detract from the usefulness of the results. For example, the results would be directly applicable to areas where longshore currents account for little or no return flow and where runoff is minor. The instantaneous release would mimic a pollutant spill or a periodic short-duration release from an industrial outflow pipe. The assumption of neutral buoyancy is valid for pollutants that readily mix into the water column because of similar density or those that are hazardous at very minor concentrations (such as PCB's) and are perhaps suspended in the water column.

Objectives

The objective of the thesis is to improve the ability to predict the fate of a pollutant released in a narrow channel under the conditions described above. This has been achieved by developing suitable numerical models which predict pollutant dispersion scenarios for various channel conditions. Numerical models have been developed which incorporate hydrodynamic components

(describing the movement of water) and dispersion components (describing the movement of the pollutant in the absence of a current) for one-dimensional situations.

Section 1.3 outlines previous work related to tidally forced pollutant transport and, to some extent, flushing processes in channels and harbours. Chapter 2 presents the theory behind the transport mechanisms at work, and develops closed-form solutions for the hydrodynamic components of the numerical model. Chapters 3 and 4 respectively discuss the numerical and physical models undertaken. Chapter 5 compares the results obtained from Chapters 3 and 4 and discusses the influence of various parameters important to transport. Chapter 6 presents an overview of the research conducted and provides some considerations for further study related to this topic.

1.3 Review of Pollutant Transport

Tidal Motions

In the Pacific Northwest, tidal forcing is a primary mechanism for the disposal of effluent from coastal channels. A typical high tide exchanges a significant portion of the volume contained within the channel at slack tide (tidal volume). This is also related to the tidal prism - the proportion of the new water entering a channel compared to its tidal volume.

In this region, tides are primarily diurnal mainly mixed (i.e. unequal tidal highs and lows with a 12 hour period). From a modelling viewpoint, it is difficult to define a characteristic tidal cycle. To determine a characteristic tidal flushing sequence one might be obliged to model a full lunar tidal cycle. This of course would represent a period much greater than the residence time of most small channels. In Nece's model studies of tidal transport in harbours (1984), three tidal ranges were used to characterize transport variations:

1) neap tides
2) mean tides
3) spring tides

Another consideration relates to seasonal variations in local tributaries, i.e. large spring and autumn fluctuations in river outflow, which will influence the residence time of effluents.

For a two-dimensional case, Nece (1984) describes the importance of gyres on the flood tide and how they will influence the mixing process. Here, it seems necessary to assess the efficiency of turbulent mixing processes because the effectiveness of tidal flushing is dependent on the rate at which the tidal flow mixes with the channel water. This, however, is not an easy task and some researchers prefer to use a more general approach.

Van de Kreeke (1983) explores harbour-related tidal exchange through the assumption that "currents induced by the wind, tide and density ... cause the waters in the basin to be completely mixed at all times". Within this context he describes residence time and flushing time for discrete and continuous dye injections in tidal prism models. He concluded that the amount of time required to expel the majority of the pollutant (residence time) for this completely mixed case is a function of two dimensionless parameters:

1) the fraction of the flood volume that is new water (i.e. tidal prism)
2) the phase of the tide at which discrete injections are released

This approach (i.e. assuming completely mixed conditions) neglects the temporal importance of mixing to the exchange process, but the tidal prism method does appear to provide a reasonable first approximation for estimating residence times.

Wind and Wave Effects

The effects of wind on mixing within a semi-enclosed body of water are much more limited than in open water conditions. Within the context of this thesis, it is assumed that wind-driven waves are of no consequence due to the sheltered nature of the case described. The wind forcing will of course control the motions of the surface layer and of floatables such as oil slicks. Schwartz and Imberger (1984) concluded that wind strength (as opposed to basin geometry relative to wind

direction) is the dominant factor controlling surface mixing. Wind shear will dictate the degree of stratification in channels with fresh water sources. Furthermore, wind shear may cause tilting of stratified interfaces and seiching effects when fluctuations in the wind shear forces occur.

By nature, waves travelling through the seaward boundary do not frequently affect mixing further upchannel. Effectively, the source of wave action to be considered is that associated with vessel motions within the channel. These forcings will not affect flushing but they may induce spatial mixing. Depending on the channel depth relative to wave length, a wave's orbital motion may cause resuspension of benthic material or simply aid in suspending non-buoyant material until it is flushed out.

Environmental Effects Related to Pollutant Transport in Harbours

In Washington State, regulations require that in the design of a channel, consideration is given to the effects on juvenile salmon that migrate along the shorelines' shallow reaches (Nece, 1972). Within the confines of some local harbours, pollutant concentration levels reached toxic levels for the vulnerable salmon fry. Other single entrance designs occupied the entire breadth of shallow zones and forced salmon fry to enter deep water areas where they fall prey to larger fish. In order to prevent this, multi-entrance channels and detached breakwaters are now favoured over single entrance enclosures to increase overall pollutant transport rates.

In Australia, regulations require that potential impact to the water quality from such dredged harbours and channels be assessed prior to construction (Schwartz and Imberger, 1986). A local concern is the accumulation of seagrasses in these enclosures. Large amounts of organic material may grow in the semi-stagnant waters within channels, drastically reducing oxygen levels (i.e. imposing a high B.O.D.) as the material decomposes. Fish kills are related to the presence of these 'dead zones' where mixing is poor and pollutant concentrations and low oxygen levels reach lethal levels. These are most commonly found at the end of long reaches. It is therefore important that channel and harbour designs avoid creating such zones.

It should be noted that regular tidal exchange within harbours and channels is beneficial to the surrounding waters by allowing local organisms to adjust to the relatively dilute effluent. If concentrated 'slugs' of polluted water exit the channel or harbour on an intermittent basis then the mortality rates of local species would be expected to increase.

Physical Models and Design

The question remains as to whether it is more effective to model pollutant mixing and transport by means of numerical models or physical models. In reviewing the literature, such as Nece (1984), it seems that economical computer models that suitably incorporate velocity fields with diffusive effects, did not exist at that time. Numerical models generally require well-defined boundary conditions in order to determine the importance of various input parameters. Physical models are well suited to determine the relative importance of these parameters since each variable can be altered to study its influence on the system.

Nece (1984) describes further physical models of harbours, with which he studied the influence of a number of aspects such as:

1) entrance orientations, widths, and locations,
2) various channel geometries (breadth:length ratios)
3) the effect of rounding basin corners.

Nece's primary interest in conducting these tests was to determine those variables important in maximizing the overall tidal exchange to the large tidal range in the Pacific Northwest. Model studies were then compared to field studies for existing small-boat harbours, and results were presented in terms of spatially averaged tidal exchange coefficients (i.e. the degree of flushing relative to harbour width and length).

Field Studies

Schwartz and Imberger (1986) describe, in detail, field studies conducted within a large marina (moorage for 1000 vessels). Using an extensive field program, they quantified a vast array of

physical parameters. Flushing rates of Rhodamine dye were compared to those described by the tidal prism method to determine the relative importance of the tide (with tidal range of approximately 1 *m*). Stratification within the layers was a prominent feature of this study and was affected to a large degree by wind shear conditions. During some ebb tides, the presence of internal supercritical flow within the constriction of the channel entrance was noted.

In this particular case, it was concluded that the dominant flushing mechanism was infiltration of fresh groundwater that aided in the mixing of the deeper stratified layers, thereby increasing the effective flushing rates. Bienfang (1980) noted a similar occurrence where groundwater infiltration increased flushing rates by a factor of six to ten. These cases show that seemingly obscure factors may turn out to be dominant for specific sites.

The field studies of Nece and Richey (1972) dealt with tracking miniature drogues that floated at different subsurface heights. Other larger surface drogues were observed as they drifted around the channel during ebb tides. These results (shown as spatial pathlines) were compared to small scale physical models.

The cited works indicate that there are various methods of approaching the subject of tidally forced pollutant transport. There is no consensus as to the best means of predicting residence times of conservative pollutants (i.e. those that do not decay) or other associated parameters. While some authors choose to assume that mixing occurs instantaneously, others dedicate entire field studies to the subject.

Chapter 2 - Theory

As described earlier, the problem of numerically modelling pollutant transport in tidal situations can be divided into two components:

1) Hydrodynamic
2) Advection/Diffusion (or Dispersion) Transport

The governing hydrodynamic equations shall be developed separately from the pollutant transport equations and give rise to the flow velocities and water elevations within the channel. However, the pollutant transport equations are governed by fluid motion and hence, require the hydrodynamic solutions within their own development.

Figure 2.1 provides definition sketches describing the notation used herein. A channel of constant average depth, d, and length, λ, is closed at one end, $x = \lambda$. The channel has a width, w, and pollutant enters the channel at position x_p. The tidal wave is described using an amplitude A, length L, celerity c, and wave period T (= L/c). The surface elevation is denoted as η.

The assumption of one-dimensional flow considerably simplifies the pollutant transport problem. As mentioned previously, variable-width one-dimensional channels provide a way of predicting flows by assuming that flows in one direction (commonly the x direction) are of orders of magnitude larger than those in other directions (the y and z directions). Much research has been conducted on fluid flow and transport mechanisms in two- and three-dimensional situations and these involve complex solutions that are still based on simplified boundary conditions. As the boundary conditions become more structured and case specific, the equations to the hydrodynamic and transport components become increasingly difficult to solve.

2.1 Governing Equations

Figure 2.1 provides definition sketches of the situation being considered.

Hydrodynamic Equations

Incompressible fluid flow in three dimensions is described by the Navier Stokes equations and the continuity equation given below (e.g. Sarpkaya and Isaacson, 1981).

Equations of motion

$$\frac{\partial U}{\partial t} + U\frac{\partial U}{\partial x} + V\frac{\partial U}{\partial y} + W\frac{\partial U}{\partial z} = \frac{1}{\rho}\frac{\partial}{\partial x}(p + \rho gz) + \upsilon\nabla^2 U \qquad [2.1]$$

$$\frac{\partial V}{\partial t} + U\frac{\partial V}{\partial x} + V\frac{\partial V}{\partial y} + W\frac{\partial V}{\partial z} = \frac{1}{\rho}\frac{\partial}{\partial y}(p + \rho gz) + \upsilon\nabla^2 V \qquad [2.2]$$

$$\frac{\partial W}{\partial t} + U\frac{\partial W}{\partial x} + V\frac{\partial W}{\partial y} + W\frac{\partial W}{\partial z} = \frac{1}{\rho}\frac{\partial}{\partial z}(p + \rho gz) + \upsilon\nabla^2 W \qquad [2.3]$$

where $\nabla^2 U = \frac{\partial^2 U}{\partial x^2} + \frac{\partial^2 U}{\partial y^2} + \frac{\partial^2 U}{\partial z^2}$

Continuity Equation

$$\frac{\partial U}{\partial x} + \frac{\partial V}{\partial y} + \frac{\partial W}{\partial z} = 0 \qquad [2.4]$$

where U, V, and W are the velocity components in the x, y, and z directions, respectively; ρ is the fluid density; g is the gravitational constant; p is the fluid pressure; and υ is the kinematic viscosity of the fluid.

Assumptions

A number of assumptions may be made in order to reduce the governing equations to a simpler form so as to apply to a one-dimensional channel. First, the tidal wave amplitude, A, is assumed to be sufficiently small compared to depth so that nonlinear terms in the governing equations can be

neglected. Secondly, the tidal wave length, L, is assumed to be significantly greater than the water depth, d, so that the vertical particle accelerations may be neglected. In addition, energy dissipation terms, including viscous effects giving rise to bottom frictional resistance and wind stress effects, are neglected. Finally, the channel is assumed to have a constant average depth and a constant average cross-sectional area, $\bar{A}_r$.

Thus the assumptions made are that:

1) $A << L, d$
2) $L >> d$
3) no friction
4) constant $\bar{A}_r$, i.e. $V = 0$

By applying these assumptions to the equations of motion and omitting the nonlinear terms, [2.1] to [2.4] reduce to:

$$\frac{\partial U}{\partial t} = -\frac{1}{\rho}\frac{\partial p}{\partial x} \qquad [2.5]$$

$$\frac{\partial W}{\partial t} = -\frac{1}{\rho}\frac{\partial}{\partial z}(p + \rho g z) \qquad [2.6]$$

$$\frac{\partial U}{\partial x} + \frac{\partial W}{\partial z} = 0 \qquad [2.7]$$

These represent the x and z momentum equations and the continuity equation, respectively.

Dispersion

The conservation of mass for the pollutant gives rise to the following governing equation:

$$\frac{d(A_r C)}{dt} = \frac{\partial (A_r C)}{\partial t} + \frac{\partial (U A_r C)}{\partial x} = \frac{\partial}{\partial x}\left(D A_r \frac{\partial C}{\partial x}\right) + K_d C + q \qquad [2.8]$$

where C is the depth-averaged and width-averaged pollutant concentration, A_r is the cross-sectional area of the channel, D is an eddy diffusion coefficient, K_d is a decay coefficient applicable to non-conservative pollutants, and q are source/sink terms (Koutitas, 1970).

Assumptions

In the present context, the sink/source terms are neglected so that the pollutant is introduced instantly at time t = 0. Furthermore, the diffusion coefficient, D is assumed independent of location along the channel, and finally it is assumed that the pollutant does not grow or decay (i.e. it is conservative).

By neglecting these terms, [2.8] reduces to:

$$\frac{\partial(A_r C)}{\partial t} + \frac{\partial(U A_r C)}{\partial x} = D \frac{\partial}{\partial x}\left(A_r \frac{\partial C}{\partial x}\right) \qquad [2.9]$$

This allows for variations of cross-sectional area, velocity and concentration with both x and t.

2.2 Initial and Boundary Conditions

Before solutions may be found for the hydrodynamic and pollutant transport components, the boundary conditions must be stated. In describing these, reference is made to Fig. 2.1.

Hydrodynamic

No initial conditions are necessary for the hydrodynamic components since the fluctuations of $\eta(x,t)$ and $U(x,t)$ are considered to be in a periodic steady state. The relevant boundary conditions in the vertical direction are:

$$W = \frac{\partial \eta}{\partial t} \quad \text{at} \quad z = 0 \qquad [2.10]$$

$$p = 0 \quad \text{at} \quad z = 0 \qquad [2.11]$$

$$W = 0 \quad \text{at} \quad z = -d \qquad [2.12]$$

These are respectively the kinematic and dynamic free surface boundary conditions at the still water level, and the kinematic boundary condition at the seabed. The free surface boundary conditions are applied at $z = 0$ rather than $z = \eta$ on the basis of the linearization entailed in the long wave theory deriving from the assumption $A << d$.

Further boundary conditions required at the seaward and landward extents of the channel ($x = 0$ and λ, respectively). Open-water tidal fluctuations are assumed sinusoidal and may be described by:

$$\eta_S = A \cos(\omega t) \qquad \text{for } t \geq 0 \qquad [2.13]$$

where η_S is the water elevation outside the channel, ω is the tidal angular frequency and A is the tidal amplitude. The water level at the seaward boundary is taken to be equal to the open-water tidal water level:

$$\eta(0,t) = \eta_S \qquad [2.14]$$

At the landward boundary ($x = \lambda$) the fluid velocity is taken to be zero:

$$U(\lambda,t) = 0 \qquad [2.15]$$

Dispersion

The initial condition for an instantaneous point discharge of pollutant at location x_p in a channel with a zero ambient concentration is:

$$C(x,0) = \begin{cases} 0 & \text{for } x \neq x_p \\ C_o\, \delta(x) & \text{for } x = x_p \end{cases} \qquad [2.16]$$

Herein $\delta(x)$ is the Dirac delta function and C_o is given as:

$$C_o = \frac{M}{\rho A_r} \qquad [2.17]$$

where M is the mass of the pollutant discharged. The Dirac delta function is defined such that:

$$\int_{-\infty}^{+\infty} \delta(x)\, dx = 1 \qquad [2.18]$$

At the initial time, the concentration corresponds to an impulse of zero width and total pollutant mass, M. The boundary condition at the landward boundary is such that the pollutant concentration gradient here is zero, so that the pollutant cannot be transported through the boundary walls. Thus:

$$\frac{\partial C}{\partial n} = 0 \qquad \text{at} \quad x = \lambda \qquad [2.19]$$

where n is the distance normal to the solid boundary (i.e. along x).

At the seaward boundary (x = 0), the boundary condition is such that the pollutant flux gradient here is zero (and inflow concentrations are zero) (Koutitas, 1970).

$$D\frac{\partial C}{\partial x} - UC < 0 \qquad \text{at} \quad x = 0 \qquad [2.20]$$

Furthermore, the concentration here is equal to the open water ambient concentration, so that there is no diffusion of pollutant through the seaward boundary toward the channel. As already indicated, this is taken to be zero, so that:

$$C(x,t) = 0 \qquad \text{for} \quad x \leq 0 \qquad [2.21]$$

2.3 Development of Hydrodynamic Component

The hydrodynamic component developed herein provides the current velocity, U(x,t) and water level, $\eta(x,t)$ at various positions and times within the channel in terms of the following parameters:

1) average water depth, d
2) channel length, λ
3) tidal amplitude, A
4) tidal period, T

A closed-form solution to the hydrodynamic equations for the case of interest may be developed using linearized long wave theory (e.g. Sarpkaya and Isaacson, 1981). On the basis of the

previous assumptions, the horizontal particle acceleration is invariant with depth and by virtue of [2.6] the fluid pressure is hydrostatic:

$$p = \rho g (\eta - z) \qquad [2.22]$$

Substituting this into [2.5] provides:

$$\frac{\partial U}{\partial t} + g \frac{\partial \eta}{\partial x} = 0 \qquad [2.23]$$

This implies that horizontal velocity is uniform over depth, $U = U(x,t)$. By integrating [2.7] from $z = -d$ to $z = \eta$, applying the boundary conditions [2.10] to [2.12] and assuming that $\eta << d$, we obtain:

$$\frac{\partial \eta}{\partial t} + d \frac{\partial U}{\partial x} = 0 \qquad [2.24]$$

[2.23] and [2.24] can be combined to form the following second order equations given in terms of a celerity, c.

$$\frac{\partial^2 \eta}{\partial t^2} - c^2 \frac{\partial^2 \eta}{\partial x^2} = 0 \qquad [2.25]$$

$$\frac{\partial^2 U}{\partial t^2} - c^2 d \frac{\partial^2 U}{\partial x^2} = 0 \qquad [2.26]$$

where:

$$c = \sqrt{g d} \qquad [2.27]$$

Equation [2.25] is commonly referred to as the wave equation. The general solutions to [2.25] and [2.26] are of the form:

$$\eta = f_1 (x - ct) + f_2 (x + ct) \qquad [2.28]$$

$$U = f_3 (x - ct) + f_4 (x + ct) \qquad [2.29]$$

which correspond to the superposition of two steady wave forms propagating at a speed c, one in the positive x-direction, and one in the negative x-direction. If both $\eta(x,0)$ or $\eta(0,t)$ are known, then the subsequent motions for all times can be determined. Because the boundary condition, [2.14] is harmonic, [2.28] and [2.29] can be expanded to:

$$\eta = a_1 \cos(kx - \omega t) + a_2 \cos(kx + \omega t) + a_3 \sin(kx - \omega t) + a_4 \sin(kx + \omega t) \quad [2.30]$$

$$U = c_1 \cos(kx - \omega t) + c_2 \cos(kx + \omega t) + c_3 \sin(kx - \omega t) + c_4 \sin(kx + \omega t) \quad [2.31]$$

where $k = 2\pi/L$, $\omega = 2\pi/T$, and a_n and c_n are constants which may be determined for the landward and seaward boundary conditions.

The derivative of [2.30] with respect to x and the derivative of [2.31] with respect to t can now be substituted into [2.23]. This produces a relationship between a_n and c_n.

$$c_1 = a_1 \alpha, \quad c_2 = -a_2 \alpha, \quad c_3 = a_3 \alpha, \quad c_4 = -a_4 \alpha \quad [2.32]$$

where $\alpha = gk/\omega = g/c$. By applying the landward and seaward boundary conditions [2.14] and [2.15], expansions for a_n may be developed as:

$$a_1 = a_2 = \frac{A}{2} \quad [2.33]$$

$$a_3 = a_4 = \frac{A}{2} \tan(k\lambda) \quad [2.34]$$

By substituting [2.33] and [2.34] into [2.30] and [2.31] respectively, the closed-form solution may finally be developed as:

$$\eta(x,t) = A \cos(\omega t) [\cos(kx) + \tan(k\lambda) \sin(kx)] \quad [2.35]$$

$$U(x,t) = \frac{gA}{c} \sin(\omega t) [\sin(kx) - \tan(k\lambda) \cos(kx)] \quad [2.36]$$

The closed-form solutions for η (x,t) and U (x,t) obtained here have a considerable advantage in not contributing to any approximation errors which arise in the finite difference methods subsequently employed in solving for the advection/diffusion components (described in Chapter 3).

2.4 Dimensional Analysis

Finally, it is useful to carry out a dimensional analysis for the concentration, C, in order to establish those parameters which influence the problem at hand. The concentration may be taken to depend on the following independent variables which define the problem:

$$C(x,t) = f(x,\ x_p,\ t,\ t_o,\ d,\ \lambda,\ T,\ A,\ g,\ D,\ C_o) \qquad [2.37]$$

A dimensional analysis then provides the following relationship between dimensionless parameters:

$$\frac{C(x,t)}{C_o} = f\left(\frac{x}{\lambda},\ \frac{t}{T},\ \frac{x_p}{\lambda},\ \frac{t_o}{T},\ \frac{d}{\lambda},\ \frac{A}{d},\ \frac{T^2 g}{\lambda},\ \frac{D^2}{gd^3}\right) \qquad [2.38]$$

where C/C_o is the normalized concentration; x/λ and t/T are dimensionless measures of the position and time respectively; x_p/λ and t_o/T are the position and instant of the initial pollutant discharge; d/λ is the ratio of the water depth to channel's length; A/d is the ratio of tidal amplitude to water depth; T^2g/λ is a measure of the tidal wave length to channel length ratio; and D^2/gd^3 is a dimensionless measure of the diffusion coefficient.

Chapter 3 - Description of Numerical Modelling

An initial step in the research was to develop a one-dimensional numerical model to assist in a basic understanding of the physical processes at work. The model is required to predict pollutant transport within the tidally-forced currents of a one-dimensional inlet of uniform depth and width, with no river forcing or stratification. This case is depicted in Fig. 2.1.

The numerical model is based upon the closed-form solution for the hydrodynamic component and finite difference approximations for the dispersion component. Previous one-dimensional models were not used as a basis for the research since it was intended that the process of developing such models would aid in understanding the fundamentals of tidally-forced pollutant transport.

The numerical model was written in FORTRAN and run on a VAXstation 3200 computer. Numerical results from these models were visualized using the graphics capabilities of Macintosh and Sun sparcstations computers.

Testing Procedure

The numerical model was developed in stages in order to allow for an understanding of each mechanism involved and in order to ensure the reliable development of the complete model. Firstly, the hydrodynamic component of the model was developed and tested. Secondly, within the pollutant transport component of the model, the advection and diffusion components were developed separately in order to study the nuances of numerically modelling each of these mechanisms. They exhibit different characteristics depending on the application of similar finite difference methods.

Once the features of the component models were adequately understood and tested, a complete transport model was compiled and tested for a situation involving uniform velocity (i.e. no tides); and only then was it combined with the hydrodynamic component so as to model the entire tidally-forced situation. Thus the testing procedure that was adopted is as follows:

1) hydrodynamic component	[numerical model # 1]
2) i) advection component	[numerical model # 2]
ii) diffusion component	[numerical model # 3]
iii) advection & diffusion, i) + ii)	[numerical model # 4]
3) coupled components, 1) & 2)	[numerical model # 5]

The details of each test scheme are described in Table 3.1 to 3.3. Further explanation of the variables are given in the following sections.

3.1 Hydrodynamic Component

This section of the model was based on the closed-form solution, [2.36] to [2.37], developed in Section 2.3. Since the closed-form solution is exact for the given boundary conditions, no sensitivity analyses were needed such as those conducted for the following advection and diffusion components which use finite difference techniques. The output from the hydrodynamic model provides the velocity U(x,t) and the surface elevation $\eta(x,t)$ at a series of positions and instances and was displayed in two dimensional arrays.

3.2 Advection/Diffusion Component

The governing dispersion equation [2.9] for one-dimensional variable-area pollutant transport may be simplified for cases where the width is uniform and elevation changes are small relative to the depth. Equation [2.9] then simplifies to:

$$\frac{\partial C}{\partial t} + \frac{\partial (UC)}{\partial x} = D \frac{\partial^2 C}{\partial x^2} \qquad [3.1]$$

Furthermore, if the velocity, U, is taken as uniform along the channel, then [3.1] gives:

$$\frac{\partial C}{\partial t} + U\frac{\partial C}{\partial x} = D\frac{\partial^2 C}{\partial x^2} \qquad [3.2]$$

Equation [3.2] differs from [2.9] in that the hydrodynamic component is omitted, resulting in constant volume and velocity conditions within the test section.

Finite Difference Method

The finite difference method (FDM) is one of the primary means of transforming the partial differential equations (PDE's) governing fluid flow to a predictable discrete system of linear equations. These equations may then be solved numerically at a series of discrete time steps. The accuracy of this method depends greatly on the size of the finite differences implemented. As the sizes of the discrete intervals grow, so does the discrete (or approximation) error. Conversely, as spatial and temporal spacings approach zero the finite difference scheme approaches the continuous system of the PDE's.

The schemes used herein are all *explicit* finite difference schemes, such that any value at an advanced time $t + \Delta t$ may be calculated explicitly from the known solution at time t. Explicit schemes generally suffer from the phenomenon of truncation error, suggesting that the pollutant is artificially advected or dispersed to a greater extent than is implied by the governing equations. The other type of scheme commonly employed for reducing PDE's is known as an *implicit* scheme. Implicit schemes entail the solution of unknowns within large algebraic matrices, and generally require considerable computing power.

As stated earlier, exact solutions to the governing equations for concentration are not possible, so that finite difference techniques are used to approximate the required results. The accuracy of such results depends upon two factors: the numerical scheme employed and the relative values of numerical parameters such as the time step size.

Consider a function f(x,t) at discrete values of x and t with intervals of Δx and Δt, respectively. In the simplest schemes based on forward, backward, and central differencing, the first-order derivative df/dx is approximated as follows:

Forward Differencing

$$\frac{df}{dx} \approx \frac{f(x+\Delta x,t) - f(x,t)}{\Delta x} \qquad [3.3]$$

Backward Differencing

$$\frac{df}{dx} \approx \frac{f(x,t) - f(x-\Delta x,t)}{\Delta x} \qquad [3.4]$$

Central Differencing

$$\frac{df}{dx} \approx \frac{f(x+\Delta x,t) - f(x-\Delta x,t)}{2\Delta x} \qquad [3.5]$$

A second-order derivative, d^2f/dx^2, can be approximated in a similar manner. In particular, the corresponding central difference is:

$$\frac{d^2f}{dx^2} \approx \frac{f(x+\Delta x,t) - 2f(x,t) + f(x-\Delta x,t)}{\Delta x^2} \qquad [3.6]$$

By expanding $f(x+\Delta x,t)$ as a Taylor series in terms of f(x), df/dx, etc., it can be shown that the forward and backward difference schemes listed as [3.3] and [3.4] are *first-order accurate*, with approximation errors denoted as $O(\Delta x)$. The central difference schemes [3.5] and [3.6] are *second-order accurate*, with approximation errors denoted as $O(\Delta x^2)$. For [3.3] and [3.4], this implies that as the interval Δx is halved the associated errors are halved, whereas those errors associated with [3.5] and [3.6], which are second-order accurate, are quartered.

The approximation (or truncation) errors for the various pollutant transport models may be determined through Taylor series expansions of the FDM operators contained within the transport

equations. Different combinations of finite difference operators create different truncation errors of varying magnitudes. First-order truncation errors affect the phase of the pollutant peak as it advects along the channel's length and may be referred to as *artificial advection.* Second-order truncation errors affect the diffusion of the pollutant and are referred to as *artificial diffusion.*

Higher order truncation errors are of less importance than first- and second-order errors and are more difficult to associate to physical phenomena such as advection or diffusion. It should be noted that zeroth order truncations are possible and affect the bias of the results. If this occurs for the cases in question, this would suggest that the mass of pollutant is not being conserved.

Figure 3.1 shows the finite difference scheme employed for the combined model. It is possible to produce higher accuracy terms for forward and backward differences, but as the accuracy increases so does the need for information from cells that are further away from the grid point in question.

Initial Conditions

In testing the various finite difference models developed and in the associated laboratory tests, the intent is to apply an initial condition corresponding to the instantaneous discharge from a point source. However, in the laboratory, a finite amount of time ($\approx$ 30 sec) is required to discharge the pollutant during which spreading occurred and, subsequently, there is a finite width to the pollutant cloud ($\approx$ 40 - 50*cm*) at t = 0. Moreover, numerical methods such as FDM have trouble simulating extreme gradients such as one-point spikes and Dirac functions, and rely on concentration information to be presented less abruptly over several grid points thus producing shallower concentration gradients.

For this reason, several different initial pollutant shapes were tested to determine the smallest number of points needed to accurately define the input profile. Results have been obtained for four

different initial concentration profiles (i.e. at t = 0) as sketched in Fig. 3.2. These correspond to:

1) one-point triangle
2) three-point triangle
3) five-point triangle
4) three-point rectangle

Of these shapes, the one-point triangle and the three-point triangle were rejected owing to the difficulty in modelling these numerically using first-order central differencing. This is due to their severe initial slopes in the concentration data. Even though the purpose of the research is to model instantaneous effluent releases from point sources (which would be represented by a very narrow rectangular block of pollutant within the channel), the five-point triangular solution shape adequately resembled the effluent input in the physical model and still remained a manageable size in the initial tests. Within the advection, diffusion, and advection/diffusion models a five-point triangular concentration profile is therefore used.

For the final numerical model, however, a larger point triangle was eventually used based on a grid size that was small enough model local variations concentration and also the initial pollutant cloud width within the physical model. Based on a grid size of 5 *cm* and estimating the average pollutant cloud width at approximately 45 *cm,* a nine-point triangle was finally chosen. The larger number of points reduces the possibility of problems within the numerical scheme.

3.2.1 Advection

Advection is defined as "...transport [of a pollutant] by an imposed current system..." (Fischer et al, 1982). In order to examine the case of advection alone, diffusion is considered not to occur. The corresponding governing equation is essentially [3.2] with the diffusion coefficient set to zero for the case of uniform velocity along the channel, and this is simplified to:

$$\frac{\partial C}{\partial t} + U \frac{\partial C}{\partial x} = 0 \qquad [3.7]$$

A general solution to [3.7] is:

$$C = f(x - Ut)$$

which corresponds to the pollutant concentration maintaining a constant spatial profile which moves at a speed U.

Finite Difference Method

Since the terms used in [3.7] are first derivatives, the advective process can conveniently be modelled using a forward-in-time, backward-in-space (FTBS) finite difference operator. Equations [3.3] and [3.4] are applied to the first derivatives in [3.7]. This provides:

$$\frac{C(x,t+\Delta t) - C(x,t)}{\Delta t} = -U \frac{C(x,t) - C(x-\Delta x,t)}{\Delta x} \qquad [3.8]$$

The concentration at the advanced time $t + \Delta t$ is therefore expressed as:

$$C(x,t+\Delta t) = C(x,t) - \frac{U\Delta t}{\Delta x} [C(x,t) - C(x-\Delta x,t)] \qquad [3.9]$$

$\frac{U\Delta t}{\Delta x}$ is known as the Courant number, C_r. Equation [3.9] may be rearranged as:

$$C(x,t+\Delta t) = (1 - C_r)\, C(x,t) + C_r\, C(x-\Delta x,t) \qquad [3.10]$$

Boundary Conditions

In carrying out tests on advection with a uniform velocity, the boundary conditions with respect to the hydrodynamic component are absent. A simple periodic boundary condition was then applied to the advection equation such that any pollutant which moved across the right-hand boundary of the domain in any time step, reappeared at the left-hand boundary. This implies that after one cycle, of period λ/U, the pollutant should be in its initial position with an unchanged concentration profile.

Truncation Error

From the Taylor series expansion of [3.7] the associated truncation error, E is:

$$E = \frac{1}{2}\Delta x\, U\,(1 - C_r)\frac{\partial^2 C}{\partial x^2} + \frac{1}{6}\Delta x^2\, U\,(1 - C_r)^2\frac{\partial^3 C}{\partial x^3} + \text{(higher order terms)} \qquad [3.11]$$

This suggests that artificial diffusion (from the $\partial^2C/\partial x^2$ term) and higher order errors exists for those results where $C_r \neq 1$. On the other hand, for $C_r = 1$, the FDM scheme is exact and all higher order terms are eliminated.

Numerical Tests - Effects of C_r

Since it is known that the Courant number influences the solution for the concentration (e.g. Abbott and Basco, 1989), the effects of C_r were examined by carrying out tests using a five-point triangular dye slug to represent the initial concentration and width with a channel length, $\lambda = 600$ *m*, and velocity, $U = 0.75$ *m/s* and various values of C_r. Table 3.1 shows the testing program adopted for this case.

By varying the Courant number, three different categories of results are produced.

1) $C_r << 1.0$: solutions are heavily damped and insufficiently accurate.
2) $C_r \leq 1.0$: solutions are identical or reasonably close to the exact solution.
3) $C_r > 1.0$: solutions are unacceptable or completely unstable due to strong oscillations.

Corresponding concentration profiles at the initial times and one cycle later when $t = \lambda/U$ are compared in Fig. 3.3 for 4 values of Courant number, $C_r = 0.5, 0.75, 1.0, 1.5$. As seen in Figures 3.3 (a) and (b) ($C_r = 0.50$ and 0.75, respectively), the peak amplitudes are lowered and the shape of the dye slug has changed. Note that no phase lag has occurred in either case but the heavy damping makes the results too inaccurate to be of much use. Figure 3.3 (c) ($C_r = 1.0$)

shows that the solution surface of the propagating dye slug is identical to the initial shape. This case relates to [3.10] reducing to the following:

$$C(x,t+\Delta t) = C(x-\Delta x,t) \qquad [3.12]$$

which may be seen to be equivalent to:

$$C = f(x - Ut)$$

when $C_r = 1$.

For $C_r = 1.5$, shown in Figure 3.3 (d), the returning solution surface bears little resemblance to the initial shape due to strong oscillations. The instability of this case increases as time progresses and is clearly *unstable*.

From these tests, it is clear that for a case of pure advection the Courant number should be held as close to 1.0 as possible without exceeding this limit. If C_r is likely to vary for a given situation within a predetermined range, it is better for C_r to err on the low side and have numerically damped results than to have results that are unstable.

Effect of grid size and time step

Certain aspects of the selection of the variables within the Courant number (i.e. U, Δx, and Δt) must be mentioned. Assuming that the velocity, U is specified *a priori* by hydrodynamic considerations, one must select the ratios of Δx and Δt to provide suitable values of C_r. The values of Δx and Δt should be selected to obtain results that are sufficiently accurate, but at the same time are efficient in terms of computing time and storage. It will be seen in subsequent sections that when diffusion is considered, the ability to vary Δx and Δt is greatly reduced. In a more specific case, tidal flow velocities oscillate between zero and a maximum value described in Section 2.3. This implies that the Courant number will also vary accordingly, assuming Δx and Δt are constant.

Figure 3.4 shows the test case ($\lambda = 600\ m$, $U = 0.75\ m/s$) where the Courant number is held constant at 0.75 while the grid sizes (Δx and Δt) are varied. Although C_r is held at a less than ideal

level, the FDM used returns solution shapes which approach the exact shape as the grid sizes are reduced. This implies that for values of C_r less than one, [3.8] is *convergent.* Stated otherwise, as spatial and temporal spacings approach zero, the FDM terms approach the corresponding terms of the PDE:

$$\frac{\Delta C}{\Delta t} + U \frac{\Delta C}{\Delta x} \quad => \quad \frac{\partial C}{\partial t} + U \frac{\partial C}{\partial x} \qquad \text{as} \quad \Delta x, \Delta t \Rightarrow 0 \qquad [3.13]$$

Interestingly enough, if the same procedure is applied to a case with a Courant number greater than one, the same reduction in grid size results in a decrease in stability for [3.8]. This case indicates a *divergent* nature.

3.2.2 Diffusion

The case of diffusion alone, without advection, may be examined by setting the velocity, U equal to zero in [3.2], giving rise to the simplest governing equation for diffusion:

$$\frac{\partial C}{\partial t} = D \frac{\partial^2 C}{\partial x^2} \qquad [3.14]$$

Exact Solution

An exact solution exists for this situation against which the results of the FDM may be compared. For this case, the pollutant released at t = 0 has an infinitely small width and an infinitely high concentration. The area under this initial concentration profile is described by the Dirac function. For the case of no boundaries, C ($\pm\infty$, t) = 0 and for t > 0, the closed-form solution (e.g. Fischer, 1981) is:

$$C(x,t) = \left(\frac{M}{\sqrt{4\pi D t}}\right) \exp\left(-\frac{(x-x_p)^2}{4Dt}\right) \qquad [3.15]$$

where M is the mass of the discharged pollutant at t = 0, and x_p is the position of initial discharge of the pollutant. Although the initial concentration profile used in the numerical models (with a

finite width) differ somewhat from the ideal initial condition used above, it is anticipated that this should not affect the exact solution which results after a sufficient duration.

Finite Difference Method

In contrast to the advective component which was modelled using a forward-in-time, forward-in-space operator, the first and second derivatives within the diffusion equation are most easily modelled using a forward-in-time, centred-in-space (FTCS) finite difference operator. The boundary elements are handled slightly differently and are discussed below. The FTCS operator implies that spatial information on both sides of a given grid point is needed in order to determine the concentration at subsequent time steps. Equation [3.14] is therefore approximated by using [3.3] and [3.6] and provides:

$$\frac{C\,(x,t+\Delta t) - C\,(x,t)}{\Delta t} = D\,\frac{C\,(x+\Delta x,t) - 2C\,(x,t) + C\,(x-\Delta x,t)}{\Delta x^2} \qquad [3.16]$$

Again, solving for the concentration at the advanced time C (x,t+Δt):

$$C\,(x,t+\Delta t) = \frac{D\Delta t}{\Delta x^2}\,[\,C\,(x+\Delta x,t) - 2C\,(x,t) + C\,(x-\Delta x,t)\,] + C\,(x,t) \qquad [3.17]$$

By denoting $D\Delta t/\Delta x^2$ as the dimensionless parameter γ, [3.17] may be written in the form:

$$C\,(x,t+\Delta t) = \gamma\,C\,(x+\Delta x,t) + (1 - 2\gamma)\,C\,(x,t) + \gamma\,C\,(x-\Delta x,t) \qquad [3.18]$$

Equation [3.18] indicates that the concentration at a given location at the advanced time t+Δt, depends on the concentrations at that location and the two adjacent grid points, all at the previous time step, t.

Boundary Conditions

A numerical model using a five point triangular pollutant slug is again employed to test this case. One set of boundary conditions was used to model this channel section, i.e. closed right and left-

hand boundaries:

$$\partial C/\partial n = 0 \qquad \text{at } x = 0 \text{ and } x = \lambda \qquad [2.19]$$

A closed boundary condition is achieved numerically by placing an additional numerical cell beyond the model's end, and equating the concentration in this cell to that in the adjacent (true) end cell:

$$C(\lambda+\Delta x,t) = C(\lambda,t) \qquad [3.19]$$

This technique, referred to as *mirror imaging*, allows the FDM to be applied to the end cell without modification and establishes a zero concentration gradient at the end cell, thereby satisfying [2.19]. To test the integrity of the closed boundaries the amount of pollutant injected into to the channel should remain constant. The mirror imaging technique provides this condition and satisfies the conservation of mass for the pollutant.

Truncation Error

From the Taylor series expansion of [3.14], the associated truncation error, E, is:

$$E = D\,\Delta x^2 \left(\frac{1}{6} - \gamma\right) \frac{\partial^4 C}{\partial x^4} + \text{(higher order terms)} \qquad [3.20]$$

Since the first term is of fourth order, this suggests that very little error is associated with [3.16] and that no artificial advection or diffusion (being first and second-order errors, respectively) exist within the scheme. Nevertheless, [3.20] may still be optimized for least error corresponding to $\gamma = 1/6$. For this case, [3.14] becomes fourth order accurate in space and second-order accurate in time, i.e. $O(\Delta x^4, \Delta t^2)$.

Numerical Tests - Effects of γ

The parameter γ has similar tendencies as the Courant number (Section 3.2.1) in causing the FDM to become unstable beyond a threshold value - in this case $\gamma = 1/2$ (Abbott and Basco, 1989). This value of γ, however does not provide the most accurate results for the diffusion case as

shown above. The pure diffusion case is therefore bounded by one γ value and most accurate for another. The range of γ values between 0 and 1/2 is still third order accurate in any case and as such is extremely precise when compared to the other schemes tested.

For the case of $\gamma = 1/6$ [3.18] becomes:

$$C(x,t+\Delta t) = \frac{1}{6} C(x+\Delta x,t) + \frac{4}{6} C(x,t) + \frac{1}{6} C(x-\Delta x,t) \qquad [3.21]$$

By varying γ, three categories of results are produced:

1) $\gamma = \frac{1}{6}$: results are fourth order accurate.
2) $\gamma \leq \frac{1}{2}$, but $\neq \frac{1}{6}$: solutions are stable and are third order accurate.
3) $\gamma > \frac{1}{2}$: solutions are unconditionally unstable.

Table 3.2 shows the testing procedure followed for the case of pure diffusion.

Figures 3.5 display the results of diffusing the five-point slug over time using various γ values. Although the results cannot be compared directly due to the use of various diffusion coefficients, they do show the stability of the results for a common time step and grid size. Figures 3.5 (a), (b), and (c) for $0 < \gamma < 0.5$ show an increasing amount of diffusion as γ increases. Figure 3.5 (d), for $\gamma = 0.55$, displays increasingly unstable results with time.

3.2.3 Advection/Diffusion

Now that the simpler cases corresponding to advection alone and diffusion alone have been addressed, the case of combined advection and diffusion is considered. Again, the governing equation, for the case of a uniform velocity is:

$$\frac{\partial C}{\partial t} + U\frac{\partial C}{\partial x} = D\left(\frac{\partial^2 C}{\partial x^2}\right) \qquad [3.1]$$

Exact Solution

To illustrate this case, a test series was run using FDM and compared to the exact solution (Fischer, 1981).

$$C(x,t) = \left(\frac{M}{\sqrt{4\pi Dt}}\right) \exp\left(-\frac{[\,U(x-x_p)\,]^2}{4Dt}\right) \qquad [3.22]$$

Finite Difference Method

The FDM employed here uses a forward-time, centred-in-space (FTCS) operator in a slightly altered form compared to that used in the Sections 3.2.1 and 3.2.2. In this situation, where diffusion plays a role in transporting the pollutant ahead of the advected slug, central differencing may be employed to increase the accuracy of the advection term to second-order, $O(\Delta x^2)$. This was not possible (or necessary) in a strictly advective case since the downstream cell contains no concentration information. Equation [3.1] is therefore approximated by using [3.3], [3.5], and [3.6] and provides:

$$\frac{C(x,t+\Delta t) - C(x,t)}{\Delta t} = U\,\frac{C(x+\Delta x,t) - C(x-\Delta x,t)}{2\Delta x} + D\,\frac{C(x+\Delta x,t) - 2C(x,t) + C(x-\Delta x,t)}{\Delta x^2} \qquad [3.23]$$

Combining these terms and implementing the notation C_r and γ, the governing finite difference equation is:

$$C(x,t+\Delta t) = [\gamma - 0.5C_r]\,C(x+\Delta x,t) + [1 - 2\gamma]\,C(x,t) + [\gamma + 0.5C_r]\,C(x-\Delta x,t) \qquad [3.24]$$

Stability range for γ and C_r

The stability range for γ and C_r is shown in Fig. 3.6 (after Leonard, 1979). Note that for $\gamma = 0$ the solution in unconditionally unstable. The curved upper boundary of the graph results from a linear stability analysis, LSA, of [3.24] and shows that C_r and γ can each be within their individual

threshold values and still produce unstable results when they are both present within a FDM scheme.

An additional dimensionless parameter shown in Fig. 3.6 is the Peclet number, P_e and may be now employed to describe the relative importance of advection and diffusion for a given set of conditions (Abbott and Basco, 1989). This is defined as:

$$P_e = \frac{C_r}{\gamma} = \frac{U \Delta x}{D} \qquad [3.25]$$

If the upper limits of γ and C_r are used (0.5 and 1.0, respectively) P_e attains a value of 2.0. For values of $P_e > 2.0$ advection is of primary importance, whereas for $P_e < 2.0$ diffusion is the dominant factor.

Boundary Conditions

For this test case of advection and diffusion with a uniform velocity, a five-point slug and periodic boundary conditions are again employed. As in Section 3.2.1, any pollutant which moves across the right-hand boundary of the domain in any time step reappears at the left-hand boundary. After one cycle, of period λ/U, the pollutant should return to its initial position with a concentration profile changed by the diffusion process.

Truncation Error

From the Taylor series expansion of [3.1] the associated truncation error, E, to the fourth order term is:

$$E = \Delta t\, U^2 \frac{\partial^2 C}{\partial t^2} + 2\, U\, \Delta x^2 \left(\gamma - \frac{1}{6}\right) \frac{\partial^3 C}{\partial x^3} + D\, \Delta x^2 \left(\frac{1}{6} - \gamma\right) \frac{\partial^4 C}{\partial x^4} + \text{(higher order terms)} \qquad [3.26]$$

This suggests that the error associated with [3.26] contains artificial diffusion related to $\Delta t U^2$ arising from the advection term. To minimize truncation error, one should attempt to reduce Δt as much as possible, assuming that U is uncontrollable. It is also interesting to note that the third and fourth order component of E are eliminated for $\gamma = 1/6$.

Numerical Tests - Effects of γ and C_r combined

Figure 3.7 shows the effect of varying P_e for the case of $\gamma = 1/6$. Table 3.3 shows the testing program followed. Relating to the Leonard's diagram, P_e may vary between 0.0 and approximately 3.7. One can see that the model is stable for P_e = 1.0 and 2.0 but for larger P_e values (i.e. P_e = 4.0) the numerical results begin to oscillate. For the particular values of D, U, Δt, and Δx chosen, results most closely resemble the exact solution for P_e = 2.0. Figure 3.8 shows numerical results for three γ values ($\gamma = 1/12$, 1/6, and 1/2) and various P_e values. Once more the stability of the results are seen to be governed by an upper limit relating to Fig. 3.6. It should be stressed that when dealing with advection and diffusion one is obliged to vary U, D, Δt, and Δx to obtain prescribed values of C_r and γ.

3.3 Combined Components and Extensions

The hydrodynamic, advective and diffusive components developed in sections 3.1 and 3.2 are now combined, allowing both U and A_r to vary. In the corresponding model, which represents a tidally forced one-dimensional channel, the velocity and channel cross-sectional area vary in time as the tides rise and fall. For this situation no closed-form solution is known to exist.

Equation Development

The governing equation for the corresponding model is:

$$\frac{\partial}{\partial t}(A_r C) + \frac{\partial}{\partial x}(U A_r C) = D \frac{\partial}{\partial x}\left(A_r \frac{\partial C}{\partial x}\right) \qquad [2.9]$$

For the case in question, the dispersion coefficient, D, is again assumed to be independent of its position along the channel, x/λ.

Equation [2.9] may be expanded as:

$$A_r\frac{\partial C}{\partial t} + C\frac{\partial A_r}{\partial t} + A_rU\frac{\partial C}{\partial x} + A_rC\frac{\partial U}{\partial x} + CU\frac{\partial A_r}{\partial x} = D\,A_r\frac{\partial^2 C}{\partial x^2} + D\,\frac{\partial A_r}{\partial x}\frac{\partial C}{\partial x} \qquad [3.27]$$

Expressions for the derivatives of U and A_r appearing in [3.27] may be derived from the exact solution [2.36] to [2.37]. Assuming that the channel is represented by width, w, the cross-sectional area is defined as:

$$A_r(x,t) = [\,d + \eta(x,t)\,]\,w \qquad [3.28]$$

Since d and w are constant, variations in the cross-sectional area, A_r, depend solely on the variations of the surface elevation, η. Expressions for the derivatives of U and A_r are as follows:

$$\frac{\partial}{\partial x}A_r(x,t) = w\frac{\partial}{\partial x}\eta(x,t) = Akw\cos(\omega t)\,[\tan(k\lambda)\cos(kx) - \sin(kx)] \qquad [3.29]$$

$$\frac{\partial}{\partial t}A_r(x,t) = w\frac{\partial}{\partial t}\eta(x,t) = -A\omega w\sin(\omega t)\,[\cos(kx) + \tan(k\lambda)\sin(kx)] \qquad [3.30]$$

$$\frac{\partial}{\partial x}U(x,t) = \frac{gAk}{c}\sin(\omega t)\,[\cos(kx) + \tan(k\lambda)\sin(kx)] \qquad [3.31]$$

Finite Difference Method

Again, the FDM scheme used here is the FTCS for all grid points including the landward and seaward boundaries. Equation [3.3] is employed to model the forward-in-time component, $\partial C/\partial t$, whereas [3.5] is used for the first-order central difference operator, $\partial C/\partial x$, and finally [3.6] is used to model the second-order central difference operator, $\partial^2 C/\partial x^2$.

Using the above abbreviations and implementing the FDM operators within [3.27], we obtain:

$$A_r(x,t)\ \frac{C\ (x,t+\Delta t)\ -\ C\ (x,t)}{\Delta t}\ +\ C\ (x,t)\ A_{rt}\ (x,t)\ + \qquad [3.33]$$

$$A_r(x,t)\ U(x,t)\ \frac{C\ (x+\Delta x,t)\ -\ C\ (x-\Delta x,t)}{2\Delta x}\ +\ A_r(x,t)\ C\ (x,t)\ U_x(x,t)$$

$$+\ C\ (x,t)\ U(x,t)\ A_{rx}(x,t)\ -\ D\ A_r(x,t)\frac{C\ (x+\Delta x,t)\ -\ 2C\ (x,t)\ +\ C\ (x-\Delta x,t)}{\Delta x^2}$$

$$-\ D\ \ A_{rx}(x,t)\ \frac{C\ (x+\Delta x,t)\ -\ C\ (x-\Delta x,t)}{2\Delta x}\ =\ 0$$

where the subscripts x and t denote the corresponding derivatives. Making use of the parameters C_r and γ, [3.33] may be rewritten as:

$$C\ (x,t+\Delta t)\ =\ -\frac{A_{rt}\ (x,t)}{A_r(x,t)}\ C\ (x,t)\ \Delta t \qquad [3.34]$$

$$-\frac{C_r}{2}\ [\ C\ (x+\Delta x,t)\ -\ C\ (x-\Delta x,t)\ ]$$

$$-\ C\ (x,t)\ U_x(x,t)\ \Delta t$$

$$-\ \frac{A_{rx}(x,t)}{A_r(x,t)}\ C\ (x,t)\ U(x,t)\ \Delta t$$

$$+\ \gamma\ [\ C\ (x+\Delta x,t)\ -\ 2\ C\ (x,t)\ +\ C\ (x-\Delta x,t)\ ]$$

$$+\ \frac{A_{rx}(x,t)\ \gamma\ \Delta x}{2\ A_r(x,t)}\ [\ C\ (x+\Delta x,t)\ -\ C\ (x-\Delta x,t)\ ]$$

Gathering terms with respect to the cells x+Δx, x, and x-Δx, [3.34] may be expressed as:

$$C\ (x,t+\Delta t)\ =\ \left(\gamma\ -\ 0.5C_r\ +\ \frac{A_{rx}(x,t)\ \gamma\ \Delta x}{2\ A_r(x,t)}\right)C\ (x+\Delta x,t) \qquad [3.35]$$

$$-\ \left(\frac{A_{rt}(x,t)\ \Delta t}{A_r(x,t)}\ +\ U_x(x,t)\ \Delta t\ +\ \frac{A_{rx}(x,t)\ U(x,t)\ \Delta t}{A_r(x,t)}\ +\ 2\gamma\ \right)C\ (x,t)$$

$$+\ \left(\gamma\ +\ 0.5C_r\ -\ \frac{A_{rx}(x,t)\ \gamma\ \Delta x}{2\ A_r(x,t)}\right)C\ (x-\Delta x,t)$$

Equation [3.35] may be used to solve for the concentration at an advanced time C (x,t+Δt) using a known solution at the present time t. Therefore, if the initial concentrations within the channel are known all subsequent concentration profiles may be determined.

Boundary Conditions

As described earlier, a nine-point slug is used to simulate the initial pollutant cloud from the physical experiments. Two sets of boundary conditions were needed to model this channel section and are shown in Figure 3.1:

1) Open left-hand boundary condition, $C = 0$
2) Closed right-hand boundary condition, $\partial C/\partial x = 0$

The open left-hand boundary condition was achieved numerically by placing an additional numerical cell beyond the open boundary of the model and by setting the concentration here to zero. This provides a positive concentration gradient satisfying [2.22]. i.e.

$$C(-\Delta x,t) = 0 \qquad [3.36]$$

This would equate to a physical situation of a longshore current moving the pollutant away from the channel mouth reducing it's concentration to the ambient conditions.

As stated earlier for the diffusive case (Section 3.2.2), the closed boundary is achieved by placing an additional numerical cell beyond the model's end and equating the concentration in this cell to that in the adjacent cell.

Time Step and Grid Size Considerations

As stated earlier, Δx and Δt will be given precedence over C_r, γ, and P_e when deciding which variables to hold constant. C_r, γ, and P_e are allowed to vary within the confines shown in Fig. 3.6.

Both Δx and Δt were chosen to be as small as possible to allow high accuracy and be capable of modelling the physical phenomena at hand. A second consideration is to chose Δx and Δt large

enough so that the total number of grid points and time steps do not exceed the computing capabilities available.

A time step of 1.25 *s* and a grid size of 5 *cm* (being the same order of magnitude as the channel depth) were considered sufficiently small increments to model transport and mixing processes occurring within the 1-D channel, while maximizing the computing power available. The 7.4 *m* channel is therefore modelled using 148 grid points along its length and the typical 20 minute tidal cycle is modelled using 960 time steps.

The final numerical model has been applied to the test cases studied within the physical experiments and presented in Table 4.1. The numerical results were acquired after the governing parameters were adjusted to provide the closest fit when compared to the physical case. These governing parameters are as follows:

D = variable m^2/s, $\Delta x = 0.05\ m$, $\Delta t = 1.25\ s$, C_r = variable, P_e = variable, and γ = variable

The concentration results (both physical and numerical) are shown in Fig. 5.1 for the five concentration plots (x_c = 1, 2, 3, 4, and 5) relating to the 'Base Case', over two tidal cycles.

Truncation Error

Whereas the truncation errors described for the previous cases contained only one or two variables for the first, second, and third order-terms in E, the Taylor Series expansion for [3.33] becomes extremely complicated due to the presence of the area term, $A_r(x,t)$, and the varying velocity, U(x,t) in [2.9]. The associated truncation error contains terms of zeroth-, first- and second-orders implying that conservation of mass, advection, and diffusion will all be affected to some degree within this FDM scheme. The important question is, how large are these errors and will they significantly affect the results? The general form of E is:

$$E = \frac{A\Delta t}{2!}\frac{\partial^2 C}{\partial t^2} + (UA - DA_x)\frac{\Delta x^2}{3!}\frac{\partial^3 C}{\partial x^3} + (\text{higher order terms}) \qquad [3.37]$$

Upon expansion of $\partial^2C/\partial t^2$ into a second-order spatial derivative, [3.37] is shown to contain 43 variables in the zeroth order term, 29 variables in the first-order term, 11 variables in the second-order term plus other higher order terms.

A sensitivity analysis was conducted for the grid size and time step used to determine the effects of the zeroth, first, and second-order terms on the final solution. Although conservation of mass is influenced by zeroth order terms, the effects of the 43 variables in this situation are minimal. The total mass of the pollutant within channel was altered by less than $10^{-5}\%$ during the first two tidal cycles of testing.

The first-order term was studied to determine its influence on the advective processes. Again, the 29 variables within this term only caused minor variations in the channel velocity (altering U(x,t) by less than $10^{-4}\%$ at any time). The second-order terms which influence the diffusive processes were found to alter the diffusion coefficient by less than 0.01%.

The reason that effects of such large groups of variables are so small is due to the fact that each variable is comprised of several high order derivatives of $A_r(x,t)$ and U(x,t) with respect to time and space. These derivatives have orders of magnitude ranging from 10^{-3} to 10^{-7} and when combined, produce even smaller magnitude variables. The effects of E on C (or M), U, and D are therefore not considered appreciable, but it would be unwise to believe that the solutions provided are without error.

Numerical Tests

The numerical tests run for this model used the same tidal conditions as used for the physical models which are described in the following chapter. Input data for the hydrodynamic component consisted of tidal amplitude, A, channel length, λ, average channel depth, d, and the tidal

period, T. Figure 3.9 shows the velocity variations along the channel length during various stages of the tidal cycle as depicted by the closed-form solutions for the Base Case. Input for the advection/diffusion portion of the model consisted of the pollutant input position, x_p, the initial concentration C(x,0), and the initial discharge time, t_o/T.

Figure 3.10 provides a 3-D perspective plot showing the path of the pollutant cloud in both time and space. One can see how the pollutant is transported by both advection and diffusion. The cross-sectional planes noted in this figure relate to positions within the physical models where pollutant concentrations were measured. Figure 3.11 is an elevation view of the same data presented in Fig. 3.10. The final data comparison is presented in the form of these 2-D concentration plots.

Chapter 4 - Description of Physical Experiments

The physical models for this research were used primarily to provide comparisons with numerical results by measuring and correlating values of concentration, C(x,t) and velocity, U(x,t) for the desired channel configurations. These models are then used to refine specific diffusion coefficients for each test scenario. All experiments were performed in the Hydraulics Laboratory of the Civil Engineering Department at the University of British Columbia.

Data acquisition and analysis was conducted using various computer platforms and video equipment. Velocity and concentration measurements were made at locations corresponding to points in the numerical grids of the computer programs. The number of simultaneous sampling points for a given test depended on the degree of accuracy needed and on time constraints. Since one of the limiting factors in the experimental set-up was the availability of only a single conductivity probe, each test had to be repeated several times in order to ascertain what was occurring during a given test scenario.

4.1 Testing Procedure

Figure 4.1 shows sketches of the channel used in the experiments. A pump connected to the tidal basin was used to control the channel's tidal rise and fall (flood and ebb). Tests were conducted by fluctuating the water level at the basin end of the channel/basin structure. Once the tidal flow within the channel was established, effluent was injected at location x_p and the concentration and velocity over time were recorded for a specific point x_c. The same test was then repeated measuring the concentration and velocity at a different position, x_c. The average test scenario consisted of five individual tests referred to as test segments. A complete group of these

tests segments is referred to as a test series. As shown in Table 4.1 the testing procedure for the physical experiments consisted of varying the following parameters:

1) Pollutant discharge position, x_p
2) Average water depth, d
3) Tidal period, T
4) Tidal amplitude, A
5) Pollutant discharge position in tidal cycle, t_o/T

A **Base Case** was chosen around which these five parameters were varied. This base case is as follows:

x_p = 3.5 *m*,
d = 8.0 *cm*,
T = 20 *min*,
A = 30 *mm*,
t_o/T = 0, 1, 2...(Peak Ebb) and 1/2, 3/2, 5/2,...(Peak Flood)

During the modelling process all parameters were held constant except one. The significance of this lone parameter to the pollutant transport was then studied. The extent to which the parameters were varied depended on limitations of the testing apparatus (as discussed herein).

These parameters may be related directly to the dimensionless parameters developed in Section 2.4. The observations from these tests will be discussed to a greater degree in Chapter 5 where the experimental results are compared to those from the numerical model.

4.2 Development of Apparatus

Within this section the various parts of the experimental set-up are described and related problems discussed. The instrument set-up is shown in Figure 4.2.

Test Channel

As shown in Fig. 4.1, the one-dimensional test case was modelled in a narrow, constant width, flume which is 7.35 *m* long, 0.25 *m* wide, and 0.48 *m* deep, with a large rectangular basin which

is 1.07 *m* wide, 0.91 *m* long, and 0.49 *m* deep attached at one extreme to simulate the channel mouth (x = 0). The floor of the tidal basin was lowered 16 *cm* below the floor of the channel in order to model the situation of deeper conditions offshore.

Tidal Pump

The pump configuration consisted of a variable speed peristaltic pump controlled by an input voltage from a signal generator which produced sinusoidal voltages of the necessary amplitude and frequency. The maximum pumping capacity (13*l* / min.) provided an average drawdown rate of 3 *mm* /min. which determined the upper velocity limit for the test series. For example, the 20 minute period chosen for the base case provides a maximum tidal amplitude of 30 *mm* and a subsequent maximum based on A and T.

During the test procedure pumping rates were found to fluctuate significantly due to the deterioration of the flexible pump tubing. The abrasiveness of the pump head on the tube would partially collapse the tube walls during testing, thereby reducing flow rates. Furthermore, small pieces of abraded tube (made of a synthetic gum rubber) dropped into the pump head, slowing down the rotating mechanism.

As a result, regular calibration was necessary to determine the actual pumping rate for a given output signal (delivered from the signal generator). These fluctuating flow rates complicated the task of reproducing each test segment within a series five times. The tidal water flowing to and from the tidal pump passed through a series of diffuser tubes to ensure a uniform velocity profile in the flume.

The original pump diffuser apparatus - a single 12.5 *mm* dia. tube - caused jetting and undesired current patterns within the basin and channel. To alleviate this problem, flow was channeled - via eight 5 *mm* tubes - to two horizontal rows of plexiglass tubing placed one atop the other and approximately 10 *cm* apart. Each of the tubes was perforated with 3 *mm* dia. holes every 20 *mm*

along its length. The two tubes were placed deep enough within the basin to avoid surface shearing but high enough to by-pass the deeper layer responsible for the upwelling at the channel's lip. To further ensure a nonstratified flow, the diffuser apparatus was placed behind a permeable membrane (or buffer) made of perforated plywood covered with horsehair matting.

Effluent Outflow Device

The effluent was diffused through a series of outflow tubes to minimize interference with the channel's tidal flow. Momentum effects of the inflowing liquid from a single tube interrupted flow patterns before the device was redesigned. The multiple tube array that was developed also allowed for faster effluent injection - in the order of 1.8*l* / min. of solution. The outflow tubes were arranged in a grid fashion to simulate the inflow into a cell such as was modelled by the numerical programs.

This array consisted of four tubes extending into the water column forming two rows in line with the channel and spaced equidistant from each other and the channel walls. Each tube had holes drilled every 2 *cm* along its length, oriented at 90° to the flow direction. The device allowed the longitudinal distance between tubes to be altered to allow for various input areas.

Wave Probe

The water surface elevation, η along the channel was measured using a capacitance-type wave probe. This probe was designed by the National Research Council of Canada (N.R.C.) and built at the University of British Columbia (UBC). The probe was positioned at the mouth of the channel ($x = 0$) and became an essential monitor for adjusting flowrates from the somewhat unpredictable tidal pump. A calibration of the probe was conducted only once at the outset of experimentation, but visual checks were performed daily to ensure recorded results corresponded to channel depth markings.

The initial calibration showed that a linear relationship existed between the wave probe's output voltage and the water level. A calibration factor was therefore incorporated directly into the acquisition system and results were logged as water depth in *mm* from the channel's base. Results were accurate to the nearest 0.1 *mm*.

Current Measurements

Velocity measurements were obtained by visually noting the progression of dye tracers placed in the channel at the same locations used by the conductivity probes. These traces consisted of injecting small amounts of rhodamine-wt™ dye into the channel with a syringe at mid depth. Measurements were taken every 60 seconds and the results were assumed to be representative for that time period. Once more, measurements were taken over the central portions of the channel, outside the zone of influence of the boundary layers. This process was somewhat labour intensive and carried out for certain test series (such as the Base Case) in order to allow a comparison with the numerical model.

Conductivity Probe

During the testing period, three different probe layouts were used in conjunction with the three different input positions, x_p tested. These are shown in Figure 4.3. From the voltages measured, the corresponding salt concentrations were then determined. The probe works by measuring the conductivity of the solution across a 25 micron gap between two sets of platinum wires. The conductivity probe corresponds to Type AII manufactured by Precision Instruments (Head, 1983). The four platinum wires (dia. 5 *μm*, each) at the tip of the probe are connected together in a wheatstone bridge to provide the output voltage signal. Within these tests, the accuracy of the output data was dependent on the data acquisition system (DAS) and was set at 0.0025 volts. The minimum discernible salt concentration associated with conductivity measurements within these experiments was 0.01 ppt.

The corresponding relationship between salinity and conductivity is indicated in Fig. 4.4 and may be completely described by a polynomial (Lewis, 1980). However, the relationship is approximately linear and may be described by a series of straight lines with slight changes in slope. The accuracy of this fit appears to increase as salinity approaches zero. This was beneficial since most salinity readings were less than 0.1 ppt.

The output voltage was calibrated daily using a set of standard salinity solutions of the following concentrations: 0.0, 0.1, 0.2, 0.5, 1.0, 2.0, 4.0, and 10.0 ppt. It was noted that over a period of 5 or 6 hours the probe's output voltage for a given salinity would increase. This "creep" is attributed to temperature variations caused by the instrumentation warming up. Whenever noticeable changes occurred the probe was recalibrated.

The conductivity probe was mounted at centre height within the channel to obtain a vertically - averaged concentration. The channel's central portion was least affected by boundary or shear layers.

To prevent damage to the extremely fragile probe tip, a tubular plastic housing was left in place during the experiments. This housing featured vertical slots extending the length of the contact zone of the probe. Nevertheless, the effect of this housing was to slow the flow field around the probe's tip resulting in potentially inaccurate values.

Data Acquisition System

Data acquisition was performed using a 12 bit Analog-to-Digital conversion board from Keithley Metrabyte Corporation which was installed in a IBM compatible PC. The data aquisition program was written in Quick Basic and made use of two of the eight available channels to record water level data (calibrated within the program), and conductivity voltages (calibrated at a later date), along with the time of each observation. Recording intervals were set at one second. The program

stored information in binary format which was subsequently converted to ASCII format for analysis.

Data sets from each test segment were later combined to produce data sets for each respective test series using Lotus 123 speadsheet software. These experimental results were graphed and compared visually with the numerical model. This is discussed in Chapter 6.

4.2.1 Effluent

Problems were encountered in producing a suitable neutrally-buoyant solution (specific gravity of 1.0) that could be traced using a conductivity probe. Following similar experiments described by Fischer (1981), an effluent mixture of saltwater and methanol was considered. Common house salt (NaCl, s.g. 2.17) breaks down readily in both water and methanol and provides an electrically conductive solution. The methanol (s.g. 0.79) provides a density compensation for the heavier salt. The addition of methanol poses few extra concerns since its vapour pressure is sufficiently low to neglect short-term evaporation and quantities are small enough not to pose any health risk.

Initial effluent mixtures used standard volumes and standard densities to produce a neutrally-buoyant solution. This mixture was not successful and quickly sank to the channel floor where it moved as a density flow. After some time it was discovered that the solution should be mixed using the *molar* volumes of the two liquids for the following reasons. When methanol is mixed with water, a small percentage of the methanol *dissolves* in the water thereby leaving a smaller volume than the two original liquids (but with the original mass). By using molar volumes this problem was mitigated.

Temperature Effects

Although it was known that a neutrally-buoyant solution could be calculated, some density problems still persisted. Initially, temperature variations between the effluent (normally at room temperature) and the channel water (some 5 degrees cooler than room temperature) caused the

solution to float. The solution was then kept in a cold-water bath (being the same temperature as the channel water) to equilibrate the temperature of the two liquids. During the test program, temperature effects of this nature caused several tests to be aborted.

Furthermore, the density effects of strong salt concentrations were more difficult to neutralize than those of more dilute ones. It was, therefore, decided to use a relatively dilute solution containing 10.0 parts per thousand (ppt), NaCl. Upon entering the channel, the effluents' concentrations dropped immediately to a third of the original value and rapidly decreased to approximately 1.0 ppt, NaCl. Average long-term concentrations were in the order of 0.1 ppt, NaCl or one percent of the original concentration.

Rhodamine-wt Dye

To track the effluent visually during the testing program, rhodamine-wt dye was added to the saltwater/methanol solution in small amounts. Because the amounts of dye added were extremely small, no density adjustments were made even though the specific gravity is equal to 1.14. Generally, solutions were mixed in the laboratory and their buoyancies were then tested in the channel water by visual inspection. If a solution was not neutrally-buoyant (for whatever reasons) small amounts of methanol or salt solution were then added to compensate for inconsistencies.

4.2.2 Aspects of Flow

Test Initialization

At the initiation of each test, the channel water was first cleared of residual currents by placing dividers within the channel at regular intervals. Dye droplets were added to the channel water and observed to see if movement occurred. The test series then commenced with the tidal pump proceeding through half a tidal cycle before the effluent was released. Both of these precautions were taken to ensure that all currents were due solely to the tidal pumping and that steady state conditions existed. A series of video images showing the movement of the pollutant cloud are

presented in Fig. 4.5. Once the effluent had entered the channel, little else had to be done except for measuring flow velocities and monitoring the water levels (controlled by the pump) to ensure that they were indeed correct. If not, minor adjustments were then made to the pumping rates to compensate.

Boundary Layers

A persistent difficulty with these experiments related to establishing a vertically uniform flow. Surface, wall, and bottom friction, in conjunction with the effect of the lip at the channel's mouth, and the pump's outflow configuration, all attributed to these vertical flow variations. A strong surface shear layer was reduced using liquid dish soap to reduce surface tension effects. Wall and bottom friction were kept to a minimum by scrubbing the tank's sides daily to prevent a build-up of surface scum caused by the semi-stagnant channel water and the combination of substances within the water. Typical thicknesses of the boundary layers were approximately 10 *mm* at the surface and 15 - 20 *mm* along the bottom and sides and were fairly constant throughout the range of tests performed.

The 8 *cm* lip at the channel / basin interface caused upwelling and a subsequent surface shear on flood tides. This effect was considered an unavoidable feature of the experiments. Initially, horsehair matting was placed at the entrance in an effort to prevent the shear effects but this did not alleviate the problem. Wire mesh was placed across the channel at regular intervals which helped reduce vertical variations in velocity and to induce some turbulence into the flow.

A problem related to low flow velocities was that the corrresponding Reynolds number, Re (= Ud/ν). This number, which is indicative of the extent of turbulent flow, is a function of depth, velocity and viscosity. A reynolds number of greater than Re = 10^5 is needed for a turbulent channel flow (giving us a turbulent diffusion coefficient) (Henderson, 1966). During the experiments however, the Reynolds number was generally less than 10^2.

Chapter 5 - Results and Discussion

5.1 General Observations from the Physical Experiments

Repeatability of Results

Since only one conductivity probe was available, each test was repeated five times, with the conductivity probe placed at different locations, x_c, to ascertain the concentration levels occurring throughout the channel. It was important to verify that conditions were similar during each repetition of the experiment and therefore several tests were repeated with the conductivity probe at the same location. As shown in Fig. 5.1 (corresponding to the Base Case), measurements were conducted twice with the conductivity probe at the same location, and the variations of concentration with time were noted. Although some variation does exist between the two curves, their trends and phases are reasonably similar. It is therefore assumed that a test series could be repeated with a satisfactory level of confidence and that conditions over the five repetitions did not change greatly.

5.1.1 Influence of Effluent Discharge Position, x_p/λ

$x_p/\lambda = 0.20$, 0.47 (Base Case) and, 0.73

During testing at $x_p/\lambda = 0.20$, significant portions of the effluent were quickly carried into the tidal basin during the following ebb tide where the effluent was subject to mixing and concentration levels on the following flood tides were too low to measure. This may be likened to the case of longshore drift. This location also provided the fastest initial velocities to the newly-released effluent and the shear layers in the effluent cloud for this case were less defined than in other tests.

For $x_p/\lambda = 0.47$ (i.e, the Base Case) the entire set of tests the transport of effluent was "well behaved" and no significant amounts of pollutant exited the channel within the two tidal cycles. After two tidal cycles the progression of the cloud in the seaward direction was noticeably further than towards the landward end. Ebb and flood tides were transported equally well.

Tests at $x_p/\lambda = 0.73$ (near the landward end of the channel) produced results that were much less varied than in the previous two cases since the effluent moved along the channel at a slower rate. At the slower velocities the wire mesh did not appear to aid in mixing and the dye cloud showed distinct shear layers.

5.1.2 Influence of Depth, d/λ

$d/\lambda = 0.01$ and 0.02

Most of the tests were conducted at $d/\lambda = 0.01$ (Base Case) since it was considered that the depth to length ratio should be maximized in order to approximate actual estuarine proportions. This was the smallest depth attainable without having excessive bottom and wall friction. This ratio translates well into a typical 1-D channel and allows a greater A/d ratio to be tested. Having $d/\lambda = 0.02$ modelled a situation with half of the effective length of the previously mentioned test The associated reduction in tidal amplitude meant that the effluent transport was greatly reduced. Greater depths lead to less prominent shearing and a more consistent central layer since the boundary layers thickness stayed roughly constant.

5.1.3 Influence of Tidal Amplitude, A/d

A/d = 0.09, 0.19, and 0.38 (Base Case)

Tests at A/d = 0.09 provided very little currents and the extent of transport after two cycles was approximately 2 *m* in either direction for the base conditions. The test series at A/d = 0.19 produced stronger currents and a considerably more stable effluent case. The extent of effluent transport after 2 tidal cycles was approximately 3 *m*. Due to the tidal pumping system available,

A/d = 0.38 (equalling a 3.0 *cm* tidal amplitude) was the largest A/d ratio possible for a 20 minute tidal period. Transport after 2 tidal cycles reached the channel's mouth (x = 0 *m*).

5.1.4 Influence of Tidal Period, $T^2/g\lambda$

T = 20 min (Base Case) and 40 min

Along with the other factors involved, the 20 minute tidal period provided a situation where - after 2 tidal cycles - effluent was on the verge of exiting the channel. The 20 minute period was also the longest period appropriate with respect to the overall test schedule. At T = 40 min tests (for an amplitude of 3.0 *cm*) produced flows that contained large or predominant shear layers. Tests were too long to be considered practical.

5.1.5 Influence of Discharge Time, t_o/T

Ebb, $t_o/T = 1.0$ and Flood, $t_o/T = 0.5$

In general, for $t_o/T = 1.0$ (discharging during the ebb), this situation allowed more of the effluent to enter the faster currents near the channel mouth. Although neither the flood or ebb tides exited the channel in general, mixing appeared to be more complete in the ebb case. For $t_o/T = 0.5$, (discharging during the flood) the transport of effluent upchannel on the initial stage of input caused exit time within the channel to increase slightly.

5.2 Combined Results of the Physical and Numerical Experiments

As described in Chapter 4 and shown in Table 4.1, the physical experiments consisted of eight series of tests, each simulating various tidal conditions. These tidal conditions were subsequently modelled numerically as described in Chapter 3 and the two models were then compared on the basis of concentration (and to a lesser extent velocity) information at the five conductivity stations described in Chapter 4. For the most part, comparisons were based on superimposing

concentration time histories of the measured results with several numerical results representing different diffusion coefficients, D.

Concentration Results

General observations of the two data sets suggests that the physical traces resemble numerical traces with diffusion coefficients in the range of D = 5.0 x 10^{-4} to 1.0 x 10^{-2} m^2/s. These diffusion rates are approximately one to two orders of magnitude larger than that expected on the basis of molecular diffusion suggesting that advective processes were involved. For the numerical model, several traces are shown in Fig. 5.2 to 5.7 relating to four different diffusion coefficients, namely:

D = 0.5, 1.0, 2.0, and 5.0 x 10^{-3} m^2/s

Each physical test series was compared to this set of numerical traces and the appropriate numerical trace was then chosen based on the criteria described below. These results are shown for five of the eight test series to determine the diffusion coefficient which produced the best fit for the various tidal conditions. Comparison of the physical and numerical data sets was conducted visually on the basis of the following criteria:

1) similarity of initial concentration peaks at a given station (in amplitude, phase, and duration)
2) coincidence (amplitude and duration) of flatter concentration trace sections which normally follow the initial peak

Of the five physical traces (i.e. x_C positions) for each test series, emphasis was placed on the central three traces as resemblances between the two data sets were strongest near the point of release, x_p. Moreover, comparison was based on the concentration traces over the first of the two tidal cycles used since similarities at any station diminished with time. During later tidal cycles, inconsistencies in the physical data became more pronounced (see Chapter 4).

The results of the comparison are shown in Table 5.1 which shows physical results matched to a 'best fit' diffusion coefficient. The quality of the fit is also given (rated as Good, Fair, or Poor). As an example, the comparison for Test Series 2a is described below.

Test Series 2a

In Figure 5.2, a diffusion coefficient, D = 2.0 x 10^{-3} m^2/s was chosen overall as providing the best fit between the numerical and the physical traces. Starting with the uppermost graph, x_C = 4.0 *m*, one can see that the initial peaks (t/T = 0.75) have very similar amplitudes but the duration of the physical peak extends approximately 0.4 tidal cycles, past that of the numerical peak. This suggests that the pollutant cloud was not transported away from this position during the test but remained in the vicinity of the conductivity probe. A set of secondary peaks, located at approximately t/T = 1.75, shows a somewhat slower increase in the physical concentration but similar amplitudes and phases as the numerical data.

At x_C = 3.5 *m*, the initial peak (t/T = 0) in the physical data has a somewhat lower amplitude than the numerical value due to smoothing of the physical data. The phase of the physical peak is offset due to a slow pollutant release. The secondary peaks are of comparable amplitude but differ in phase by approximately 0.25 of a tidal cycle. The physical concentration trace tapers to zero after one tidal cycle, whereas all numerical traces suggest concentration levels, C/C_O to be in the range of 0.1 to 0.3. This suggests that the pollutant cloud had been transported away from the central position and did not return.

At x_C = 3.0 *m*, two physical traces are available showing the variability between physical test results. Although curves #1 and #2 both display similar amplitudes (in both their primary and secondary peaks), curve #1 appears slightly before #2 and declines at a slower rate suggesting a longer residence time at this position. In both cases, the numerical models underestimate the duration of the primary peaks. For the secondary peaks, both physical curves exhibit the same

phase as the numerical curves but their amplitudes were less than those predicted by the numerical curves.

The quality of the fit was considered to be *good* despite the various shortcomings already mentioned. Variations in the physical results are considered to be due in part to the presence of boundary layers in the physical experiments. Furthermore, the fact that each test series is comprised of data from five separate test runs reduces the dependability of these results. The inability of the numerical model to estimate the relative duration of the physical peaks might be due to the plastic housing protecting the probe. This housing could potentially trap fluid during periods of lower channel velocities, thereby overestimating the residence time at that location. From the results, one cannot state with confidence that the pollutant cloud will be situated in a particular position at a particular time. The combination of vertical variations in velocity and vertical variations in dye concentration combine to transport the cloud either faster or slower than predicted.

One can, however, follow the progression of the primary peak downchannel in Fig. 5.2 from $x_c = 3.5\ m$ to $x_c = 3.0\ m$. At this point the tides switch from an ebb to a flood, and the pollutant cloud moves upchannel towards $x_c = 3.5\ m$ and $x_c = 4.0\ m$. For the concentration traces, one may join the primary peaks of the graphs to provide a clearer picture of how the pollutant cloud is moving along the channel with time.

A similar analysis was performed for each of the test series and the results shown in Table 5.1. Generally, initial peak amplitudes for the physical experiments at all stations were within 20% of the input concentration suggested by the numerical results. In two of the six cases, secondary physical peaks at the discharge position, $x_p = 3.5\ m$, occurred well before that predicted by the numerical models suggesting that the pollutant cloud is not transported as far as anticipated due to a slower advective process.

In several cases concentration peaks arise in the physical results where none are predicted. Conversely, in some instances physical results taper off to zero concentration, where the numerical results suggest that the pollutant cloud should be present.

Velocity Results

Velocity data consisting of results from measured dye traces and from the hydrodynamic equations were obtained for Base Case tidal conditions and are presented in a similar manner to the concentration data. As stated previously, physical velocity data consist of noncontinuous point measurements, averaged both in time and in the vertical profile of the test channel. Figure 5.8 shows the corresponding velocity information at five locations (x_C = 2.0, 3.0, 3.5, 4.0, and 5.0 *m*). Since the numerical velocity data are described by the hydrodynamic equation [2.37], using only the known parameters, no best fit analysis is required.

As shown in Fig 5.8, there is little resemblance between the two sets of data at any given position over the two tidal cycles. Although the respective amplitudes are of similar orders of magnitude, there are large discrepancies in phase and duration. Moreover, measurements of the dye tracers tended to produce sporadic results with velocities oscillating between positive and negative for each subsequent velocity reading (i.e. every 1/8 tidal cycle).

These inconsistencies are associated with variations in the vertical velocity profile generally attributed to boundary layers. The physical data obtained was therefore dependent on the depth at which the dye trace was observed. These results imply that the relative amount of advection within the two models is different and therefore would lead to variations in the transport rates as shown in the concentration data. Overall, one can see that velocities decrease in magnitude as one moves upchannel from the open channel boundary (i.e., from x_C = 2.0 to 4.0 *m*).

Overall Results

For the majority of the figures, a diffusion coefficient of 2.0 x 10^{-3} m^2/s was chosen. This represents a value greater than molecular diffusion (by approximately two orders of magnitude) suggesting that pollutant transport is therefore a function of both advective and diffusive processes.

Within the physical model the shear layers present would create larger interfaces over which molecular diffusion occurs. Generally, one would expect that the diffusion coefficient should be related to the velocities present within the channel and for tidal conditions which portray similar channel velocities, the diffusion coefficient should be the same. Within the testing program, only three different velocity conditions were tested with five of those being similar to the velocity conditions for the base case. Following this line of logic, these test series should all match to one diffusion coefficient. As seen in Table 5.1, there is no perfect agreement with this and for test series with similar velocity conditions as the Base Case (U_{max} = 0.73 *cm/s*), D ranges from 0.5 to 2.0 x 10^{-3} m^2/s.

As one can see, there is no set pattern relating maximum velocity to diffusion coefficient as anticipated. The variability in the physical results causes one to question the likelihood of making an accurate comparison.

5.3 Discussion

Using a diffusion coefficient of 2 x 10^{-3} m^2/s concentration contours are presented in Figures 5.9 to 5.12 showing the relative effect of the various tidal conditions to pollutant transport. Results are shown in terms of three of the dimensionless parameters developed in Section 2.4, namely:

1) Tidal amplitude to depth ratio, A/d
2) Initial pollutant discharge position, x_p/λ
3) Discharge time within the tidal cycle, t_p/T

Tidal amplitude to depth ratio, A/d

In Fig 5.9, the tidal amplitude to depth ratio is varied between 0.05 and 0.19. This relates to 25%, 50%, and 100% of the A/d ratio corresponding to the Base Case tidal conditions. One can see that the results vary mostly in the area affected with larger A/d ratios and that after 2 tidal cycles the width of the pollutant cloud is the same for all three cases (approximately 0.3 of the channel's length, λ).

The affected area, however, varies from 0.30 λ for Fig. 5.9 (a) to approximately 0.47 λ for Fig. 5.9 (c). Also the peak concentration at any time is identical for all three cases, again owing to identical diffusion coefficients.

Initial pollutant discharge position, x_p/λ

In Fig. 5.10, the pollutant discharge position, x_p/λ is varied between 0.20 and 0.74, corresponding to the discharge of the pollutant in regions of differing channel velocities. As seen in the figure, the range of the pollutant cloud decreases for the case of discharge positions further upstream, corresponding to lower velocities.

In the case of Fig. 5.10 (a) the pollutant cloud reaches the seaward boundary where some of the pollutant is transported out of the channel in question and does not return. The total amount of pollutant is therefore diminished and the subsequent concentration contours taper off at a faster rate than in Figs. 5.10 (b) and (c).

Discharge time within the tidal cycle, t_o/T

In Fig.5.11, the pollutant discharge time is varied for a central location within the channel. Fig. 5.11 (a) corresponds to a discharge at the peak velocity during an ebb tide (i.e, $U = -U_{max}$) while Fig. 5.11 (b) relates to a discharge on the flood tide ($U = U_{max}$). In these two case the spatial extent to which the pollutant is transported up and down-channel is approximately equal.

Chapter 6 - Conclusions and Recommendations

6.1 Conclusions

Both physical and numerical model studies have been conducted to lend insight to the subject of transport and subsequent diffusion of a neutrally buoyant effluent instantaneously released into one-dimensional tidal bodies.

Numerical model development

Several numerical models relating to various conditions of advection, diffusion, and hydrodynamic processes were developed. Within the hydrodynamic component closed-form solutions for the velocity and surface elevation are developed for this one-dimensional, tidally forced, constant depth case. These are applied in conjunction with the finite difference method (FDM) for determining pollutant concentration within the advection/diffusion components of the models. These models were studied to determine the effects of varying the primary modelling parameters: Δx, Δt, U, and D. Secondary modelling parameters (namely, C_r, γ, and P_e) are also discussed. Results are compared to exact solutions wherever possible and discrepancies are explained in terms of truncation errors associated with the numerical schemes employed.

For the cases of pure advection or diffusion, it was determined that the primary modelling parameters could be arranged to obtain results approaching exact solutions. For the advection/diffusion case, however, it has not been possible to state which mix of the primary modelling parameters would produce the best results.

One of the difficulties with the numerical model stems from Δt and Δx being assigned constant values throughout. To overcome this, the most reasonable approach appears to be to keep the Δt and Δx values as small as possible to allow the increased accuracy (due to the FDM's convergent nature) to counter the model's varying accuracy.

Physical model development

Physical models were developed and implemented on the basis of a suitable selection of the dimensionless parameters governing the situation. For a series of test conditions, pollutant concentration time histories were obtained at five locations, along with velocity measurements for selected tests. Velocity information was considered too erratic to be used as a basis for comparison to numerical results. Shear layers were present in many test cases which caused non-uniformities in the vertical direction. This implies that concentration measurements were, to some degree, depth dependent. If account is taken of vertical variation in concentration and velocity results are consistent with the numerical results. The testing procedure was considered successful overall.

Comparison of numerical and physical models

Dimensional analyses were conducted and within the numerical and physical models tested, the following factors were varied: effluent input position within the channel, x_p/λ; release time within the tidal cycle, t/T; initial water depth within the tidal cycle, d/λ; tidal amplitude to depth ratio, A/d; and duration of the tidal period, T. Concentration and velocity data from the two models were correlated to derive a diffusion coefficient for the numerical model developed. A diffusion coefficient of $D = 2.0 \times 10^{-3}\ m^2/s$ (for $\Delta x = 0.05\ m$, $\Delta t = 1.25$ s and γ and C_r both varying) provides the best match between physical and numerical data.

The final numerical model was then re-run for the selected diffusion coefficients and the effects of the dimensionless parameters were discussed. Results indicate that while tidal amplitude will determine the extent of transport within a channel, the amount of diffusion after a full tidal cycle is

similar for all cases. The transport is, however, skewed down-channel towards the seaward boundary and the skewness increases with larger tidal amplitudes. Similarly, for different input positions, the primary factor is the decrease in transport rates further up-channel.

Pollutant released near the open boundary is transported by the greater channel velocities present, thereby having the opportunity to exit the channel. Pollutant released at the landward boundary tends to remain stationary, and is acted upon only by diffusive processes. The variation in the proportion of advective and diffusive processes along the channel is, perhaps, the largest single factor affecting the transport of a pollutant within this one-dimensional situation.

6.2 Recommendations for Further Study

Numerical Modelling

Within the numerical modelling section, improvement could be made to the process by adapting the closed-form hydrodynamic solutions for the one-dimensional case to a width-varying case. The finite difference schemes used could be improved by implementing a more complicated FDM scheme such as the GREATEST scheme developed by Leonard (1979). Further study of the role of the primary modelling parameters within the advection/diffusion model would also be useful.

Physical Experiments

In the case of physical model tests, the apparatus used was well designed although the performance limitations were not anticipated. These studies could easily be continued with the addition of the necessary equipment. The channel used was a manageable size and has the possibility to provide further valid test results. A series of conductivity probes will allow the researcher to carry out a complete test without needing to repeat an experiment several times. Conductivity probe measurements would be taken at various depths within the channel to

determine the effects of stratification. A more accurate method of measuring channel velocities is also needed.

The most crucial point to further physical studies would be the acquisition of a larger capacity pump. The scope of the study was severely impeded by lesser ideal flow rates and tidal amplitudes resulting in low Re values. Stratified flows may be minimized by setting the bottom of the tidal basin flush with the channel bottom. Shear and boundary layers due to wall and bottom friction will continue to be a problem that will most easily be solved by using a larger testing tank.

References

Abbott, M. (1979) " *Computational Hydraulics - Elements of the Theory of Free Surface Flows* ". Pitman Press, Boston.

Abbott, M. and Basco, T. (1989) " *Computational Fluid Dynamics* ". Longman Scientific & Technical, United Kingdom. Ch. 3 - Ch. 5.

Bienfang, P. (1980) " *Water Quality Characteristics of Honokohau Harbour: A Subtropical Embayment Affected by Groundwater Intrusion*". Pacific Science, Vol. 34, pp.279-291.

Chu, W., Barker, B., Akbar, A. (1988) " *Modeling Tidal Transport in the Arabian Gulf* ". J. Waterway, Port, Coastal and Ocean Eng. Div., A.S.C.E., Vol.114, pp. 455-471.

Chu, W., and Yeh, W. (1985) " *Calibration of a Two-Dimensional Hydrodynamic Model* ". Coastal Engineering Vol. 9, The Nederlands, pp. 293-307.

Fischer, H., List, E., Koh, R., Imberger, J., Brooks, N. (1979) " *Mixing in Inland and Coastal Waters*". Academic Press, San Diego.

Fischer, H. (1981) " *Transport Models for Inland and Coastal Waters* ". Academic Press, San Diego.

Head, M.J. (1983) " *The Use of Miniature Four-Electrode Conductivity Probes for High Resolution Measurement of Turbulent Density or Temperature Variations in Salt Stratified Flows* ". Ph.D. Thesis, University of California, San Diego.

Henderson, F.M. (1966) " *Open Channel Flow* ". Macmillan Publishing, New York.

Koutitas, C. (1970) " *Mathematical Models In Coastal Engineering* ". Pentech Press, London.

Leonard, B.P. (1979) " *A Stable and Accurate Convective Modelling Procedure Based on Quadratic Upstream Interpolation*". Computer Methods in Applied Science and Engineering. Vol. 19 pp.59-98.

Lewis, E.L. (1980) " *The Practical Salinity Scale and Its Antecedents*". IEEE Journal of Ocean Engineering. Vol. 5, pp.3-8.

Nece, R. (1984) " *Planform Effects on Tidal Flushing of Marinas*". J. Waterway, Port, Coastal and Ocean Eng. Div., A.S.C.E., Vol. 104, pp. 251.

Nece, R., Richey, E. P. (1972) " *Flushing Characteristics of Small-Boat Marinas*". Proceedings 13th Coastal Engineering Conference. Vol. 3, pp. 2499-2513.

Sarpkaya, T. and Isaacson, M. (1981). *"Mechanics of Wave Forces on Off-shore Structures"*. Von Nostrand Reinhold, N. Y., pp. 198-202.

Schwartz, R.A., Imberger, J. (1988) " *Flushing Behaviour of a Coastal Marina*". Proceedings 21st Coastal Engineering Conference., pp. 2626-2640.

van de Kreeke, J. (1983) " *Residence Time: Applications to Small Boat Basins* ". J. Waterway, Port, Coastal and Ocean Eng. Div., A.S.C.E., Vol. 103, pp. 416-430.

Tables

C_r	U (m/s)	Δx (m)	Δt (s)	Profile #
0.5	0.5	5	5	1, 2, 3, and 4
		10	10	1, 2, 3, and 4
		20	20	1, 2, 3, and 4
0.75	0.75	5	5	1, 2, 3, and 4
		10	10	1, 2, 3, and 4
		20	20	1, 2, 3, and 4
1.0	1.0	5	5	1, 2, 3, and 4
		10	10	1, 2, 3, and 4
		20	20	1, 2, 3, and 4
1.5	1.5	5	5	1, 2, 3, and 4
		10	10	1, 2, 3, and 4
		20	20	1, 2, 3, and 4

Table 3.1 Numerical modelling testing program for a pure advection case

γ	D (m^2/s)	Δx (m)	Δt (s)	Profile #	Boundaries
0.10	0.10	5	1.25	1, 2, 3, and 4	open / closed , closed / closed
		10	5	1, 2, 3, and 4	open / closed , closed / closed
		20	20	1, 2, 3, and 4	open / closed , closed / closed
0.17	0.17	5	1.25	1, 2, 3, and 4	open / closed , closed / closed
		10	5	1, 2, 3, and 4	open / closed , closed / closed
		20	20	1, 2, 3, and 4	open / closed , closed / closed
0.25	0.25	5	1.25	1, 2, 3, and 4	open / closed , closed / closed
		10	5	1, 2, 3, and 4	open / closed , closed / closed
		20	20	1, 2, 3, and 4	open / closed , closed / closed
0.45	0.45	5	1.25	1, 2, 3, and 4	open / closed , closed / closed
		10	5	1, 2, 3, and 4	open / closed , closed / closed
		20	20	1, 2, 3, and 4	open / closed , closed / closed
0.50	0.50	5	1.25	1, 2, 3, and 4	open / closed , closed / closed
		10	5	1, 2, 3, and 4	open / closed , closed / closed
		20	20	1, 2, 3, and 4	open / closed , closed / closed
0.55	0.55	5	1.25	1, 2, 3, and 4	open / closed , closed / closed
		10	5	1, 2, 3, and 4	open / closed , closed / closed
		20	20	1, 2, 3, and 4	open / closed , closed / closed

Table 3.2 Numerical modelling testing program for a pure diffusion case

γ	Cr	Pe	D (m^2/s)	Δx (m)	Δt (s)
0.084	0.084	1.0	67.2	400	200
	0.167	2.00	67.2	400	200
	0.250	3.00	67.2	400	200
	0.333	4.00	67.2	400	200
	0.418	5.00	67.2	400	200
0.167	0.167	1.00	133.6	400	200
	0.334	2.00	133.6	400	200
	0.500	3.00	133.6	400	200
	0.584	3.50	133.6	400	200
	0.668	4.00	133.6	400	200
0.333	0.333	1.00	266.0	400	200
	0.500	1.50	266.0	400	200
	0.666	2.00	266.0	400	200
	0.745	2.25	266.0	400	200
	0.833	2.50	266.0	400	200
0.490	0.490	1.00	392.0	400	200
	0.613	1.25	392.0	400	200
	0.735	1.50	392.0	400	200
	0.858	1.75	392.0	400	200
	0.980	2.00	392.0	400	200

Table 3.3 *Numerical modelling testing program for Advection/Diffusion component with constant velocity*

Test Series	x_p, Discharge Position (m)	d, Average Water Depth (cm)	T, Tidal Period (min)	A, Tidal Amplitude (cm)	Umax, Maximum Channel Velocity (cm/s)	Discharge Time
1 a)	1.5	8.0	20.0	1.5	0.73	Ebb
b)						Flood
2 a)	3.5	8.0	10.0	0.75	0.73	Ebb
b)						Flood
3 a)			20.0	0.38	0.18	Ebb
b)						Flood
4 a)			20.0	0.75	0.36	Ebb
b)						Flood
5 a)	**3.5**	**8.0**	**20.0**	**1.5**	0.73	**Ebb**
b)						**Flood**
6 a)			40.0	3.0	0.73	Ebb
b)						Flood
7 a)		16.0	20.0	1.5	0.36	Ebb
b)						Flood
8 a)	5.5	8.0	20.0	1.5	0.73	Ebb
b)						Flood

Note: The highlighted lines refer to the **Base Case**

Table 4.1 *Physical testing programme showing variation in tidal conditions based upon x_p, d, T, A, and the discharge time.*

Test Series	x_p, Discharge Position (m)	d, Average Water Depth (cm)	T, Tidal Period (min)	A, Tidal Amp. (cm)	U_{max}, Max. Velocity (cm/s)	Diffusion Coefficient, D (10^{-3} m^2/s)	Quality of Fit
2 a (Ebb)	3.5	8.0	10.0	0.75	0.73	1.0	Good
b (Flood)						1.0	Good
3 a (Ebb)	3.5	8.0	20.0	0.38	0.18	2.0	Fair
b (Flood)						1.0 - 2.0	Fair
4 a (Ebb)	3.5	8.0	20.0	0.75	0.36	0.5 - 1.0	Poor
b (Flood)						1.0	Fair
5 a (Ebb)	3.5	8.0	20.0	1.5	0.73	0.5 - 1.0	Poor
b (Flood)						1.0	Fair
7 a (Ebb)	3.5	16.0	20.0	1.5	0.36	2.0 - 5.0	Fair
b (Flood)						2.0 - 5.0	Fair
8 b (Flood)	5.5	8.0	20.0	1.5	0.73	2.0	Fair

Table 5.1 *Best Fit Analysis comparing physical concentration traces with numerically produced traces for various diffusion coefficients.*

Figures

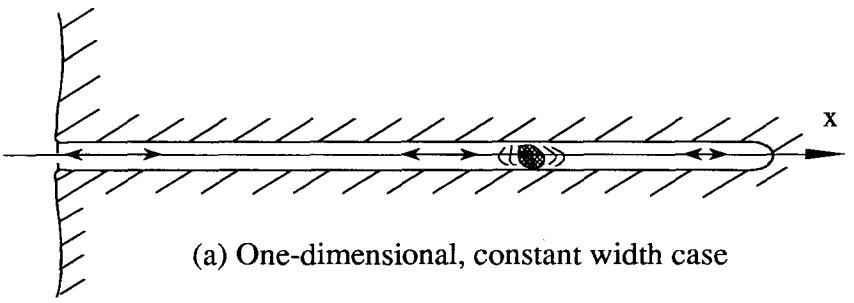

(a) One-dimensional, constant width case

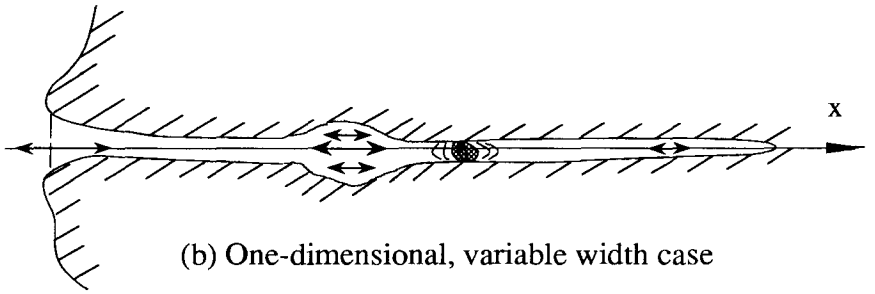

(b) One-dimensional, variable width case

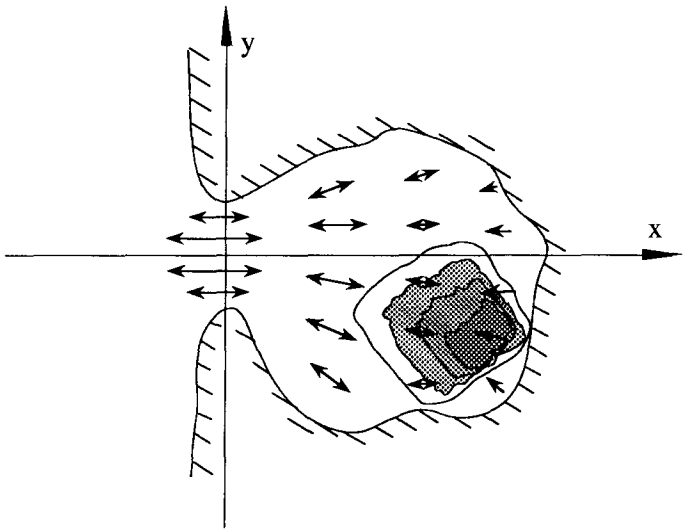

(c) Two-dimensional case

Figure 1.1 *Sketches of (a) 1-D, (b) 1.5-D, and (c) 2-D channels*

(a) tidal notation

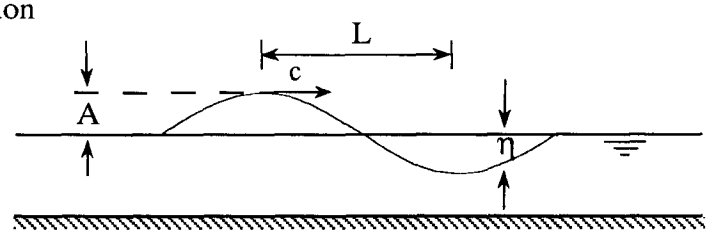

b) elevation

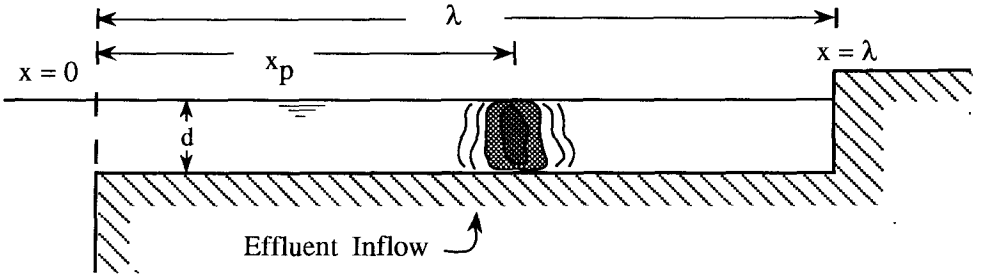

(c) plan

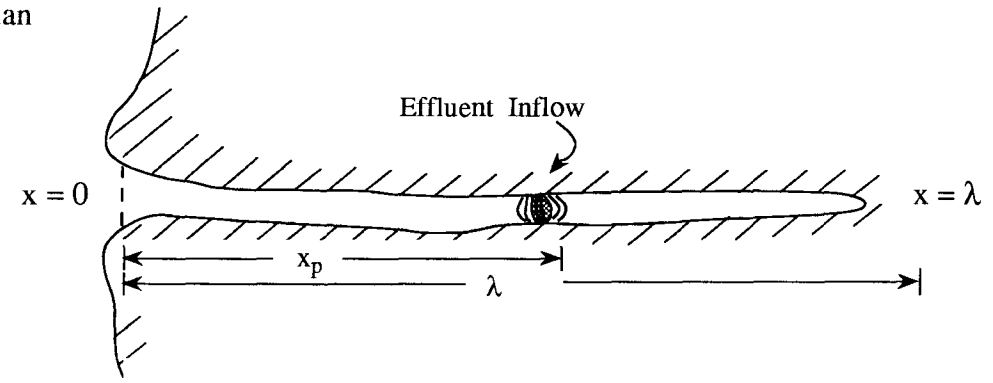

Figure 2.1 *Definition sketches of the one-dimensional situation (a) tidal notation (b) elevation (c) plan*

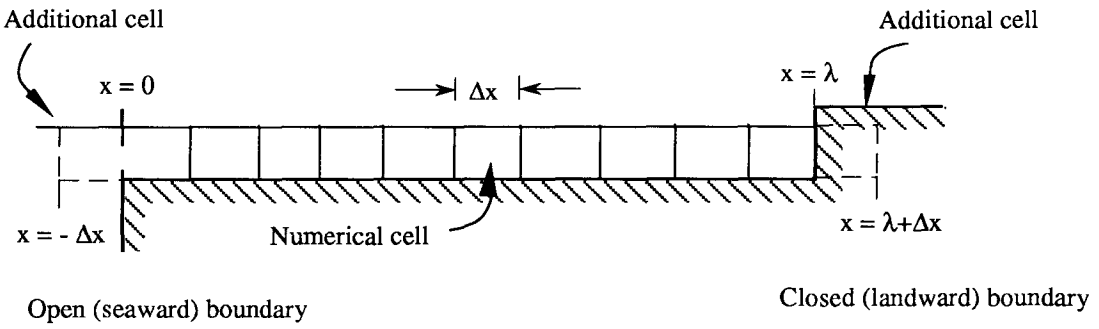

Figure 3.1 *Layout of the finite difference scheme showing boundary conditions and numerical cells*

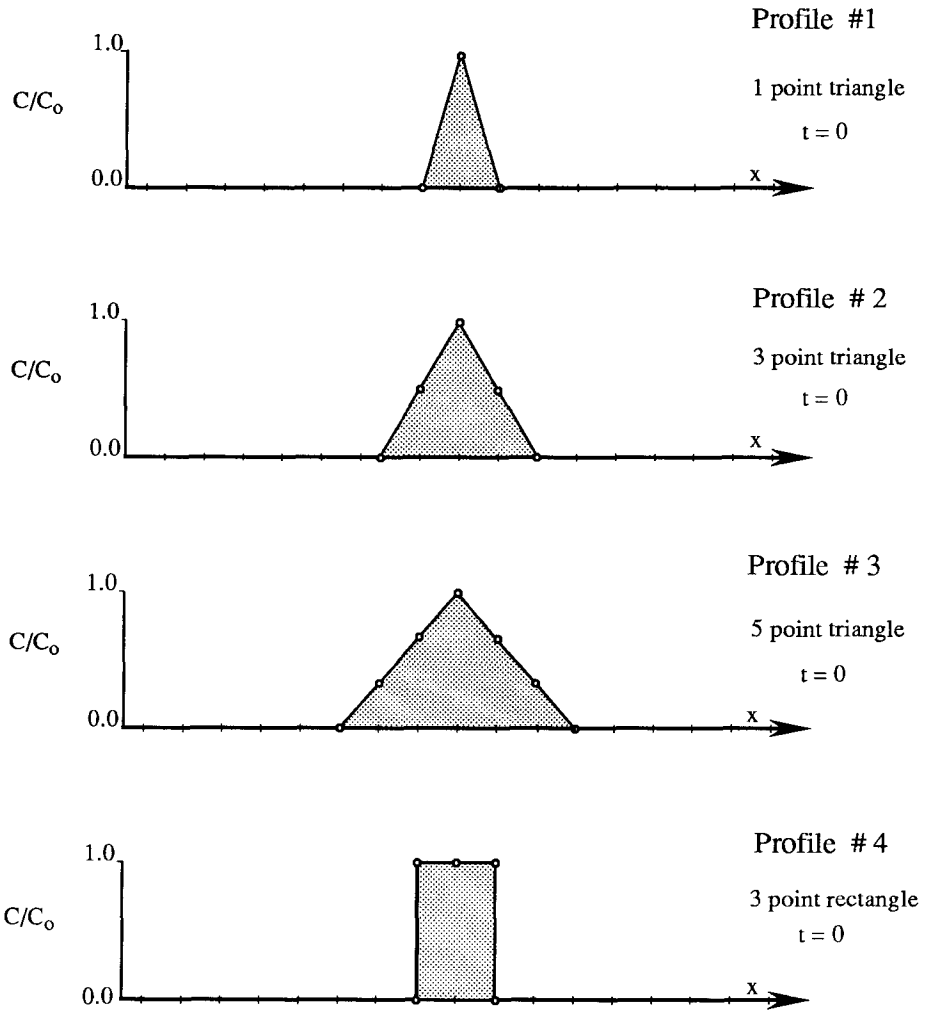

Note: the effluent for each model was equilibrated to contain a unit volume.

Figure 3.2 *Initial shapes of pollutant concentrations tested in numerical models.*

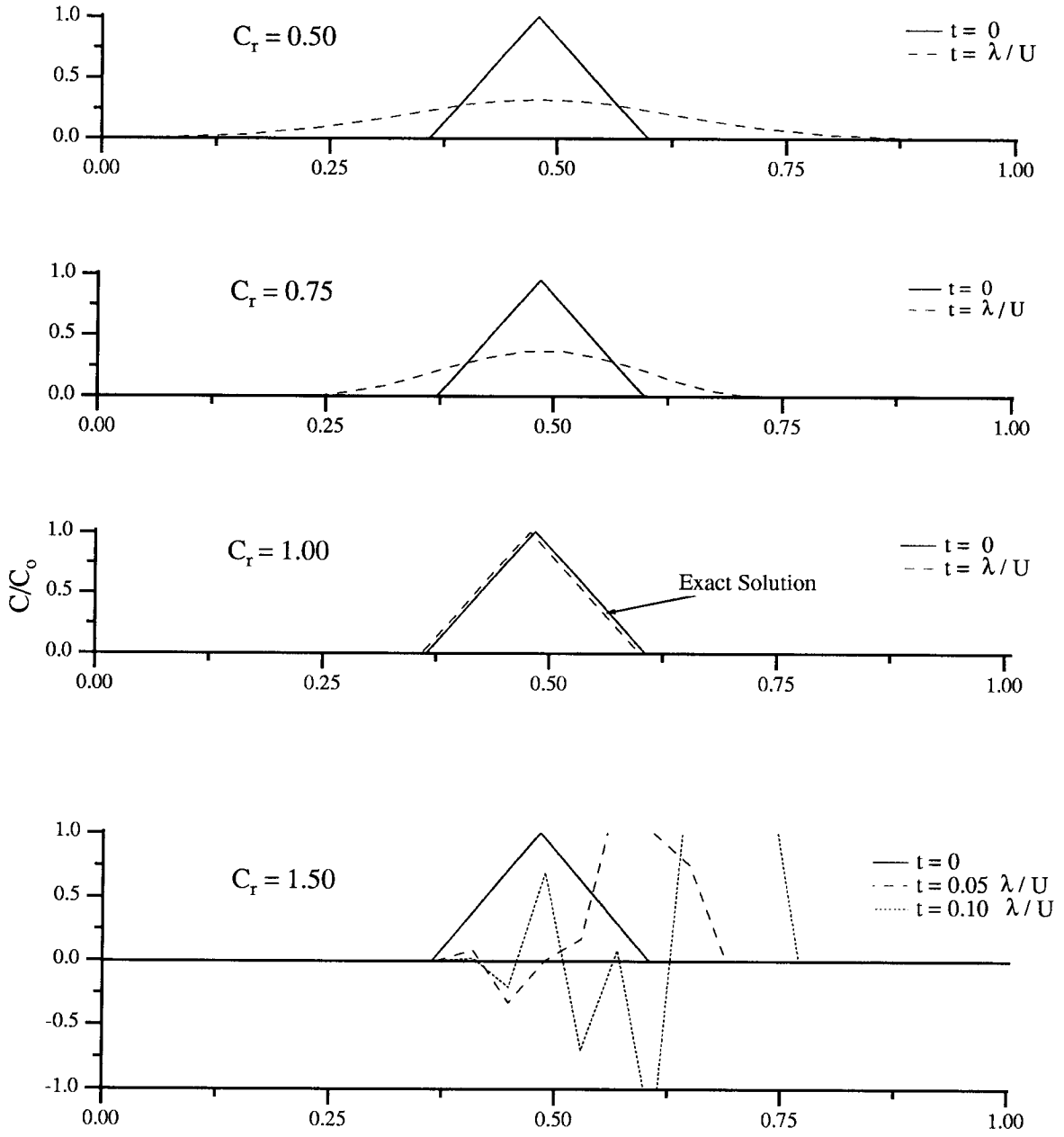

Note: λ/ U represents one tidal cycle

Figure 3.3 *Effect of varying the Courant number (= $U\Delta t/\Delta x$) within the advection model.*

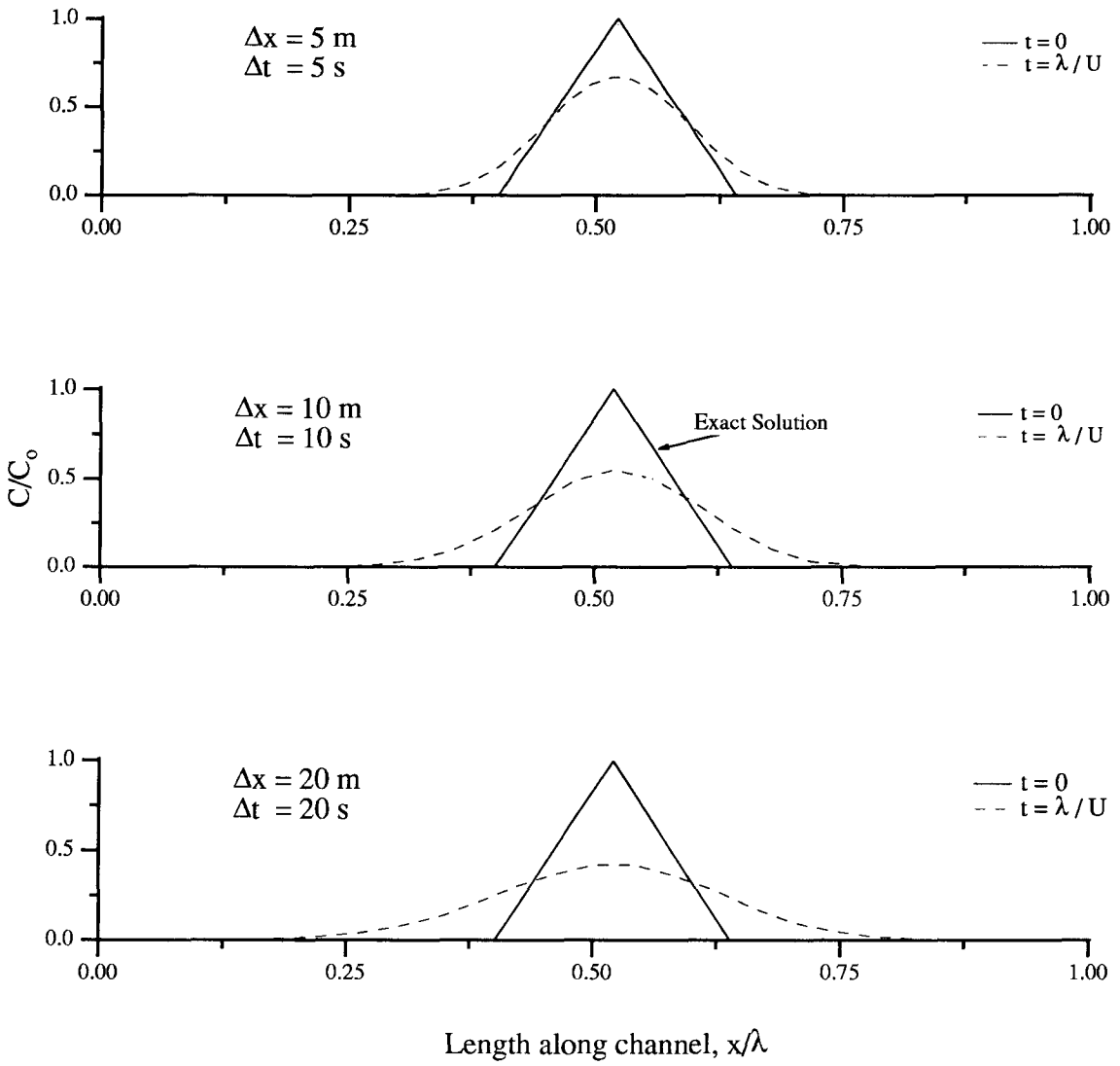

Note: λ/U represents one tidal cycle

Figure 3.4 *Effect of varying Δt and Δx while holding the Courant number (= UΔt<??>/Dx) constant within the advection model.*

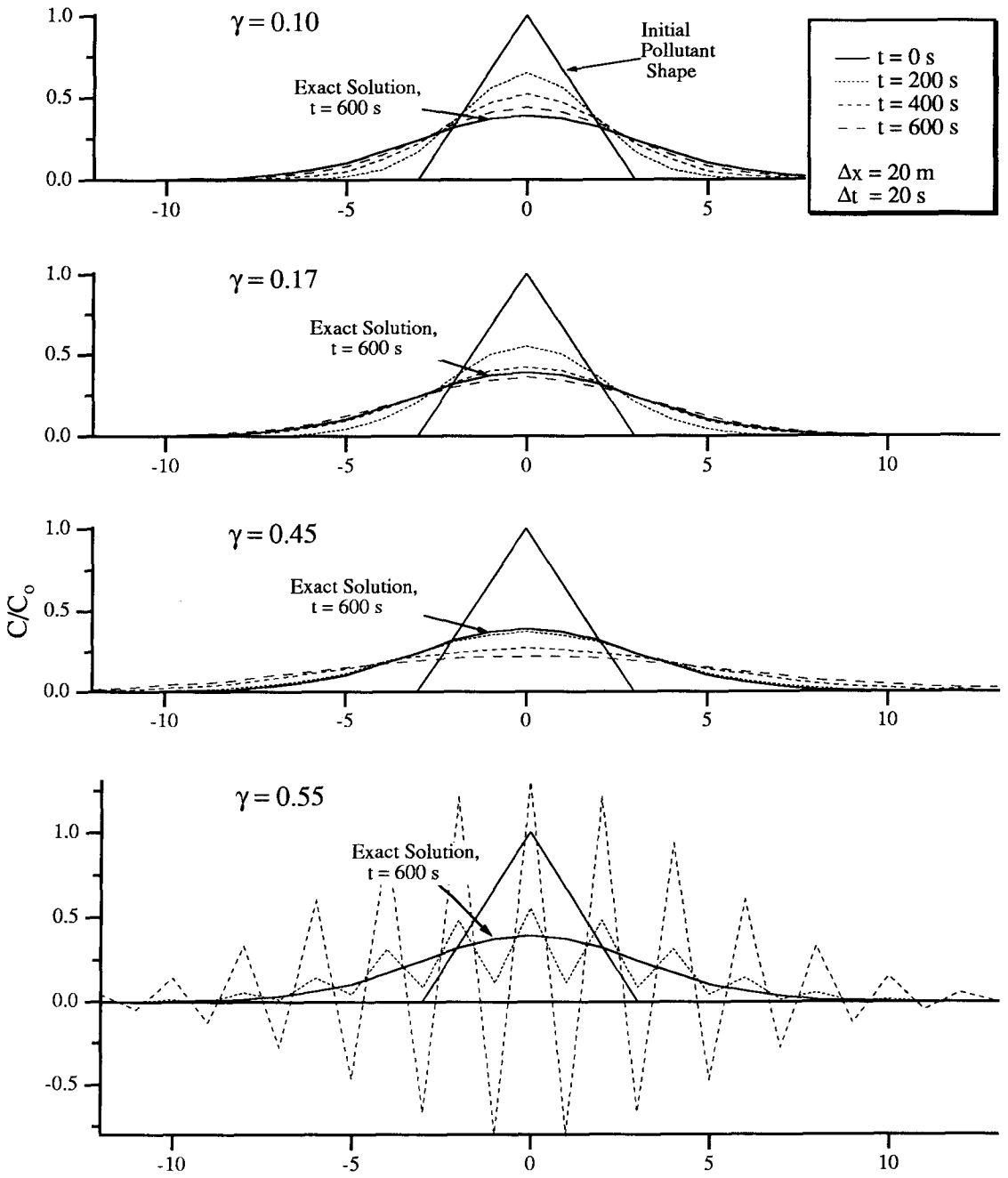

Figure 3.5 *Effect of varying $\gamma (= D\Delta t/\Delta x^2)$ within the diffusion model by varying D while holding Δt and Δx constant*

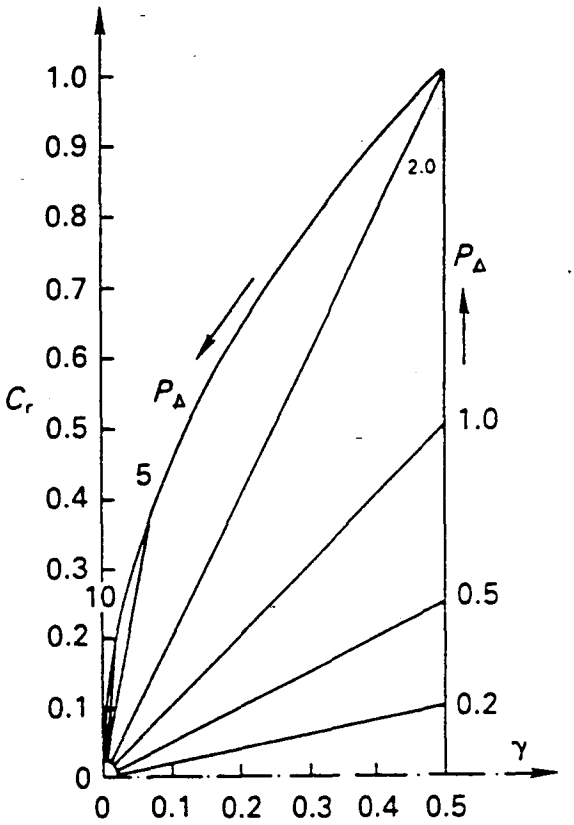

Figure 3.6 *Stability range for FTCS finite difference operator with respect to C_r and γ (after Leonard, 1979)*

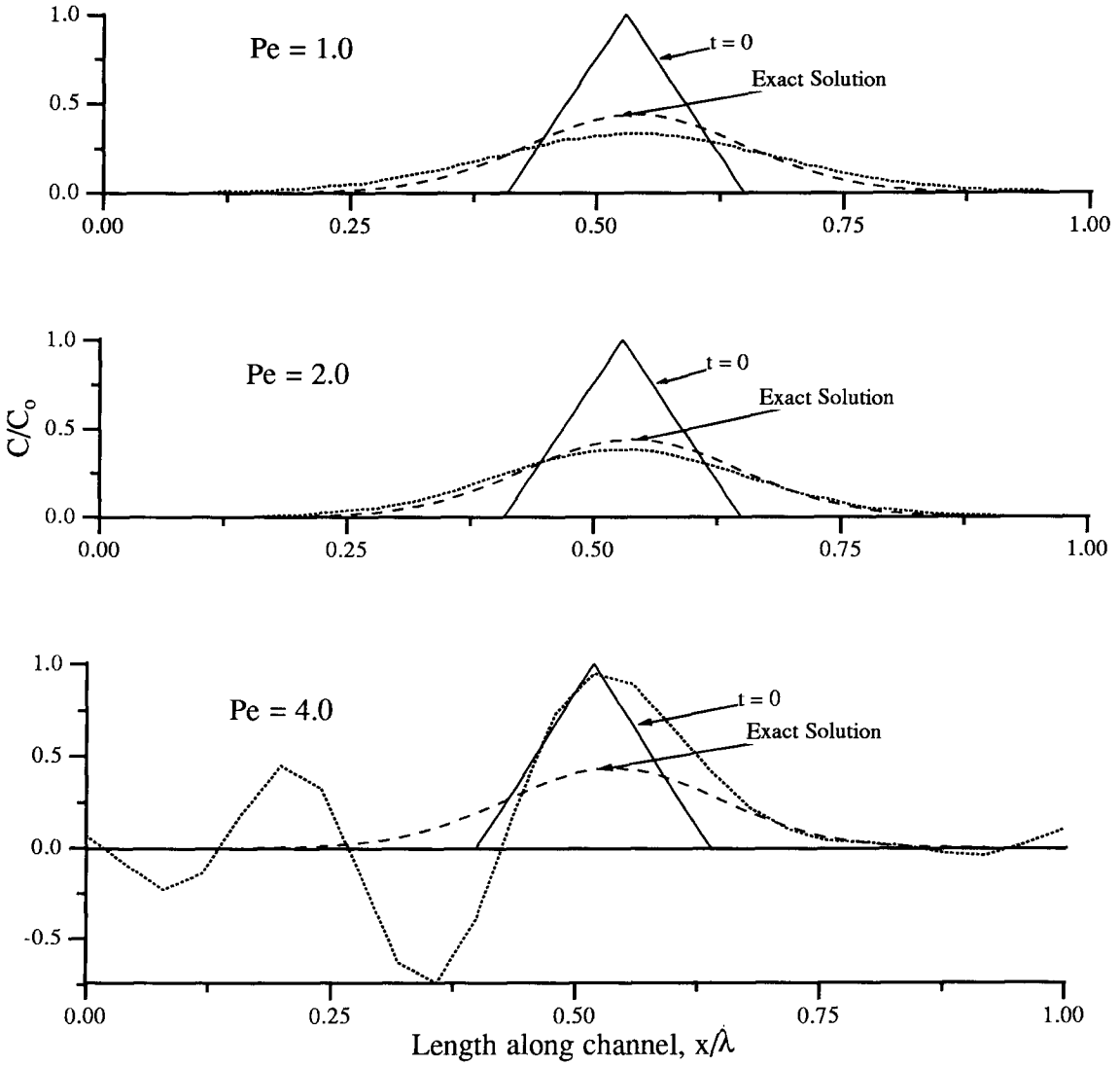

Figure 3.7 *Effect of varying P_e (= C_r/γ) within the advection/diffusion model and varying C_r, Δx, and Δt while holding γ, U and D constant*

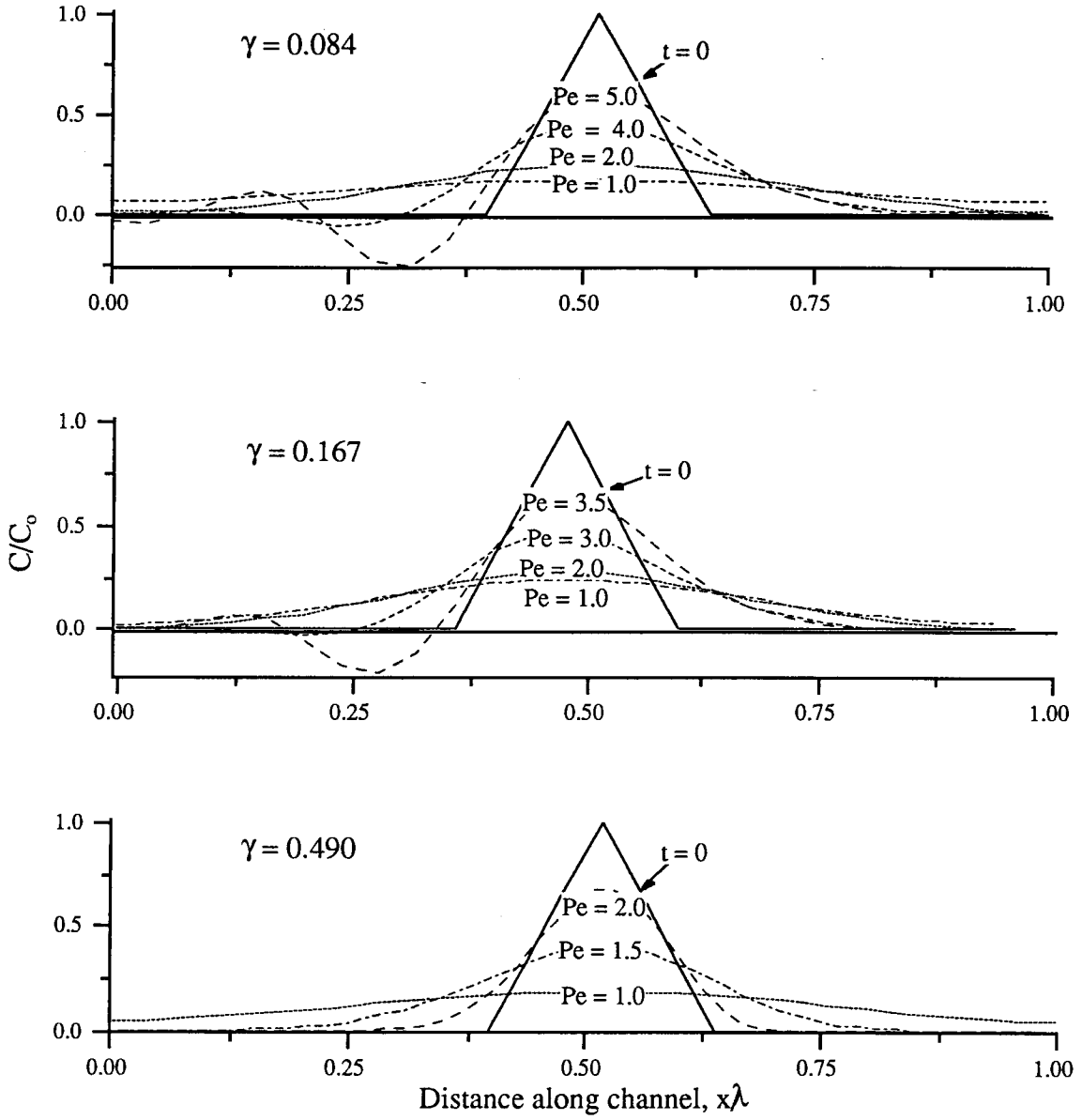

Figure 3.8 *Effect of varying $\gamma (= D\Delta t/\Delta x^2)$ within the advection/diffusion model while holding Δx and Δt constant*

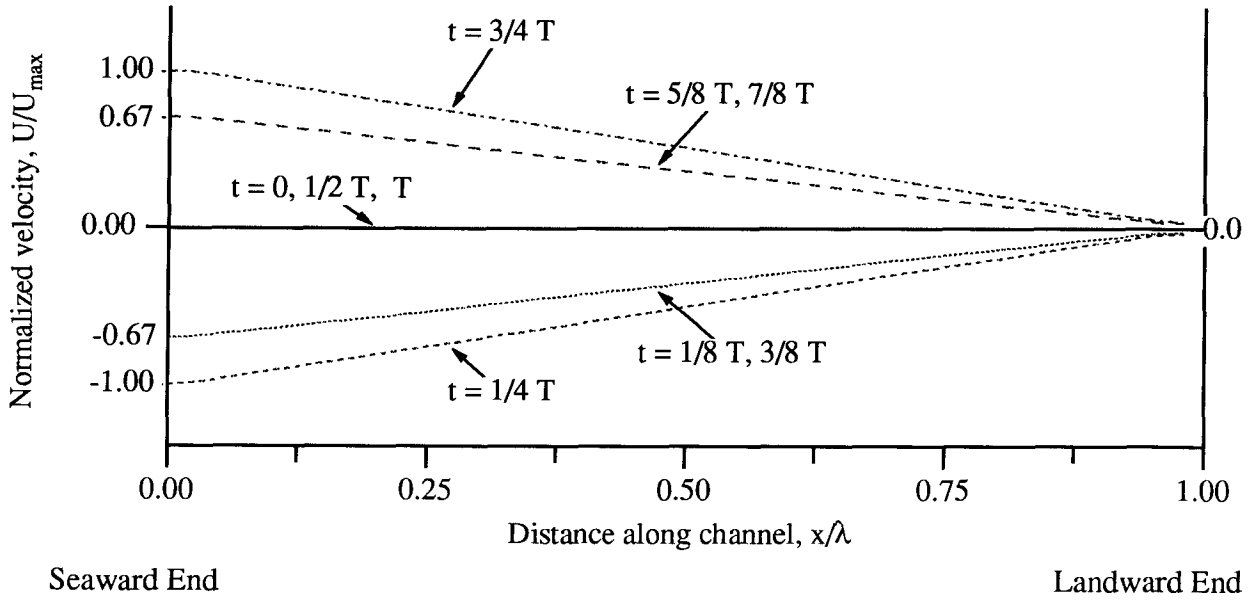

Figure 3.9 *Velocity variations along channel length during various stages of the tidal cycle as predicted by closed-form solutions for the Base Case*

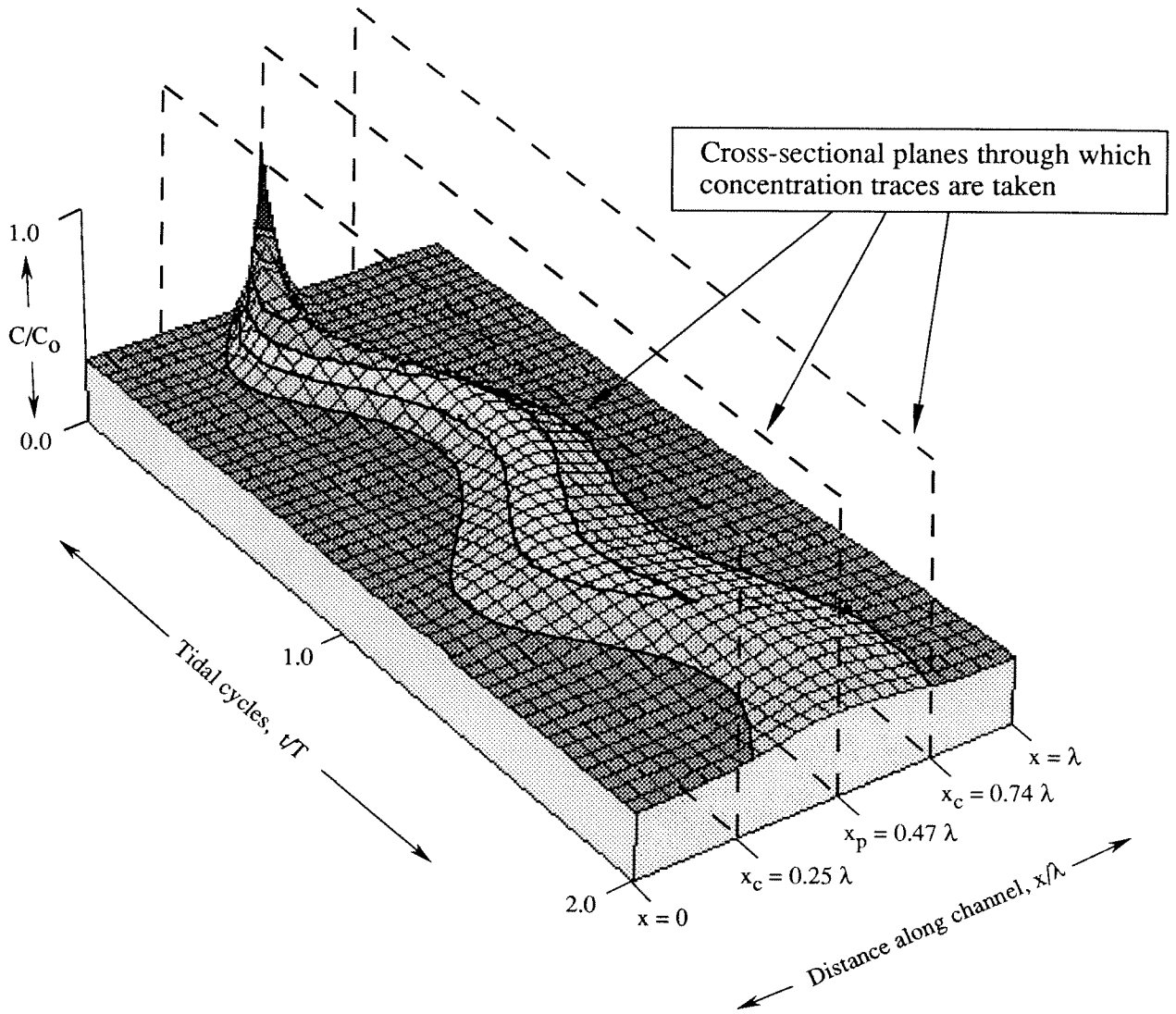

Figure 3.10 *3-D perspective plot showing path of pollutant cloud in both time and space*

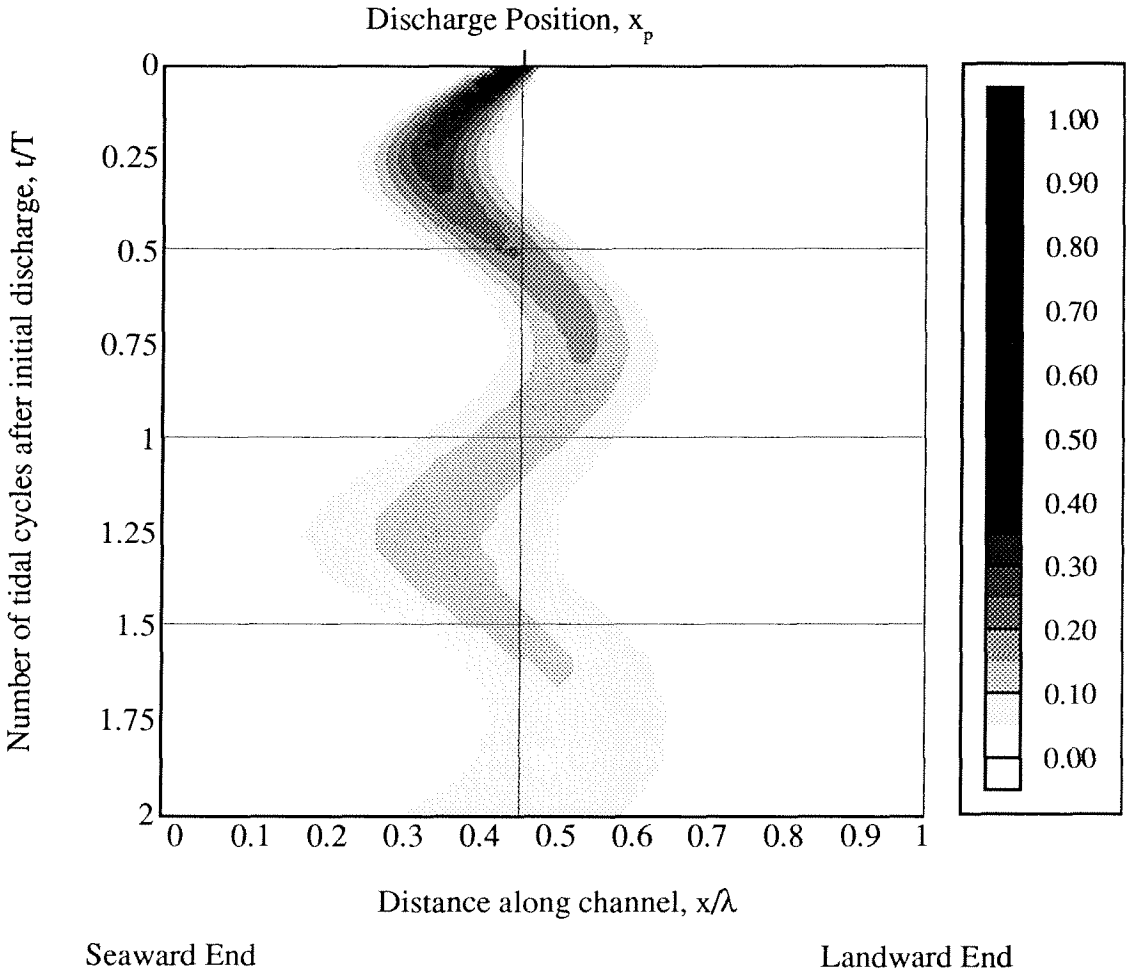

Figure 3.11 *Concentration contours in time and space for the Base Case. (Discharge on the ebb tide)*

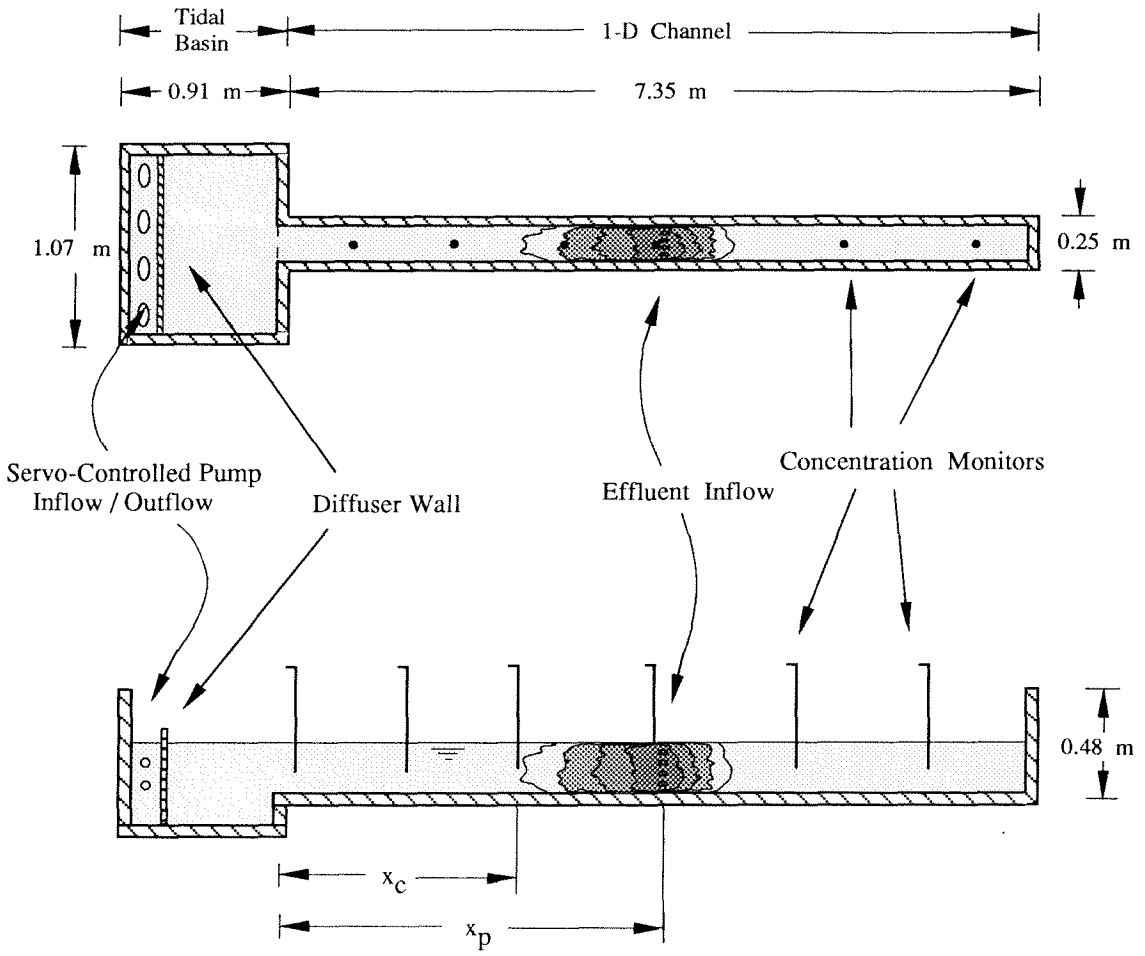

Volume Channel 0.90 m^3
Volume Basin 0.48 m^3

Figure 4.1 *Plan and elevation of channel used in the physical model studies.*

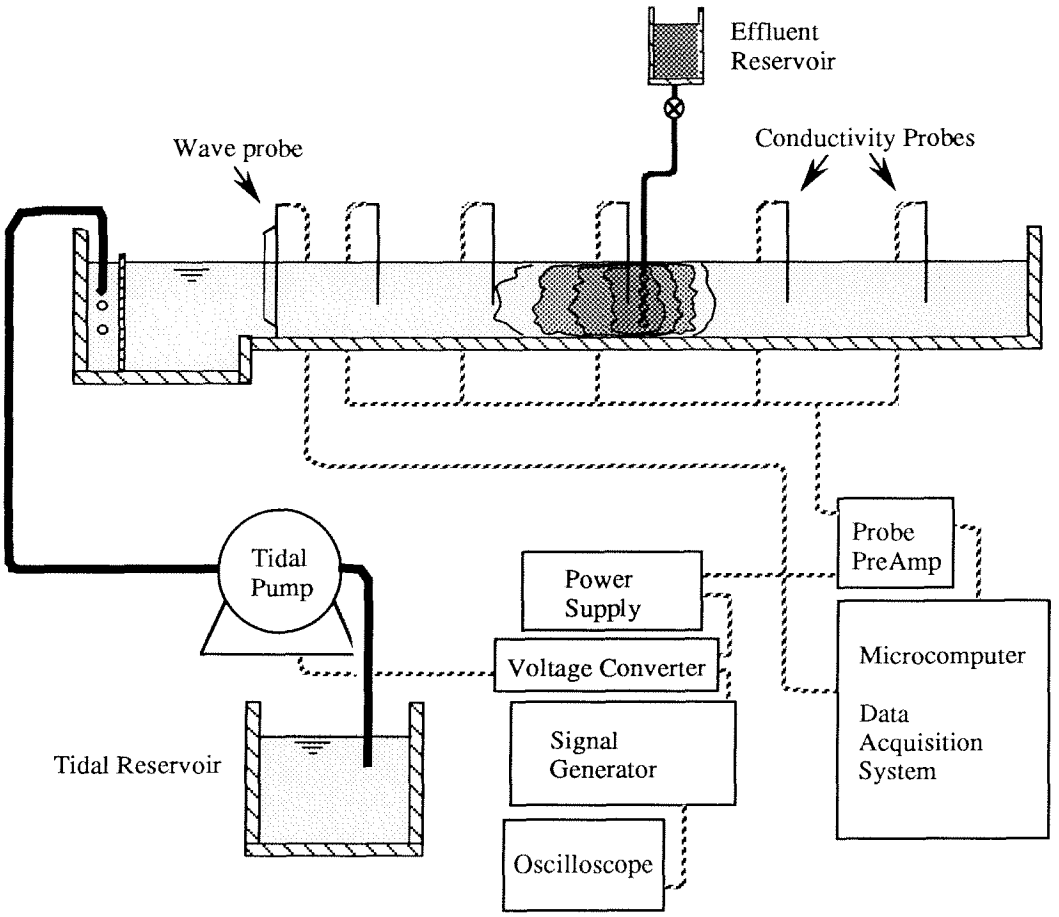

Figure 4.2 *Set-up of physical model instrumentation*

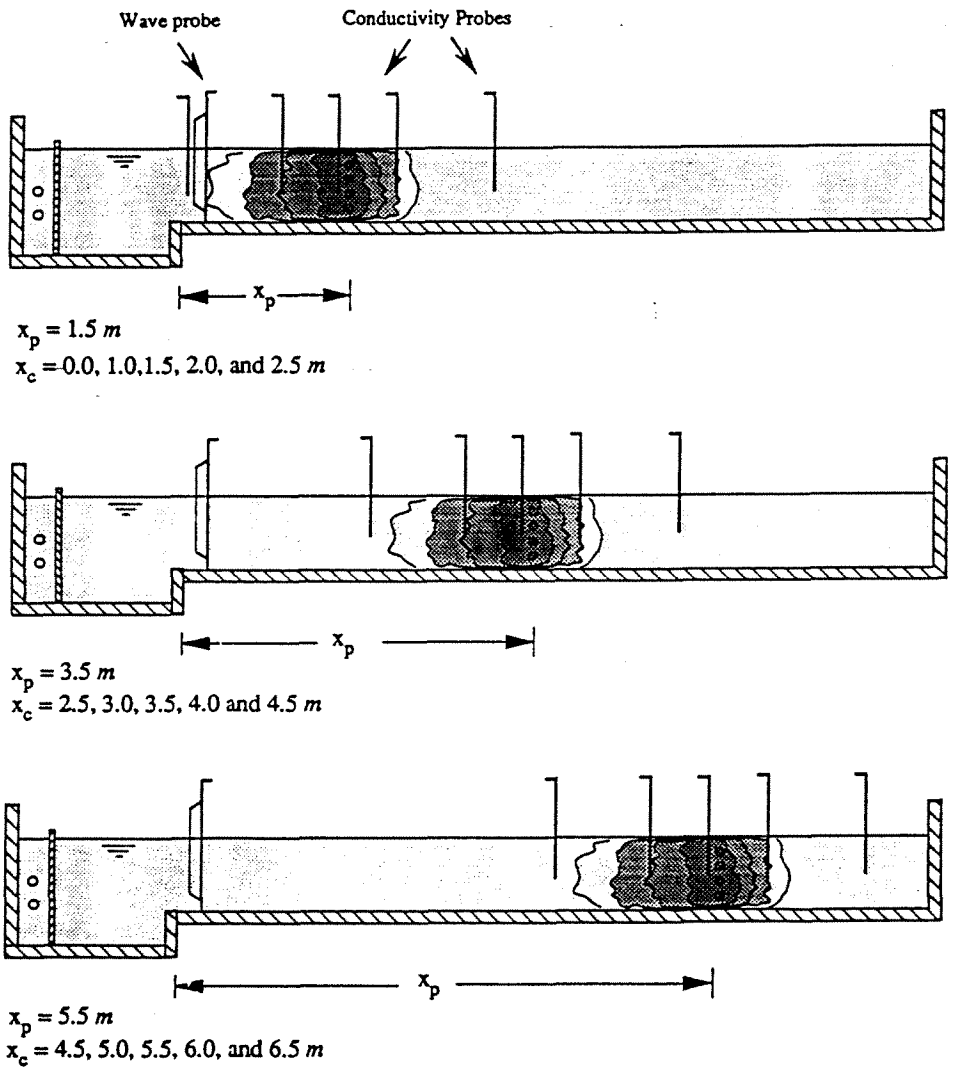

Figure 4.3 *Position of conductivity probes, x_c, in relation to various effluent input positions, x_p*

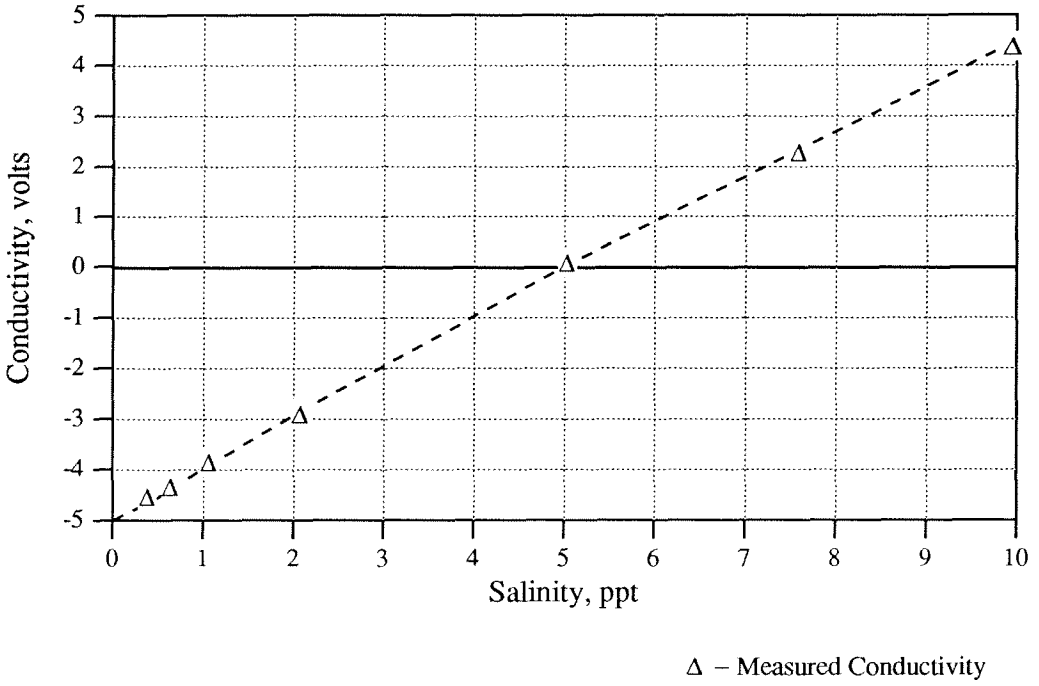

Figure 4.4 *Correlation for the conductivity probe between measured conductivity and the predetermined salinity values*

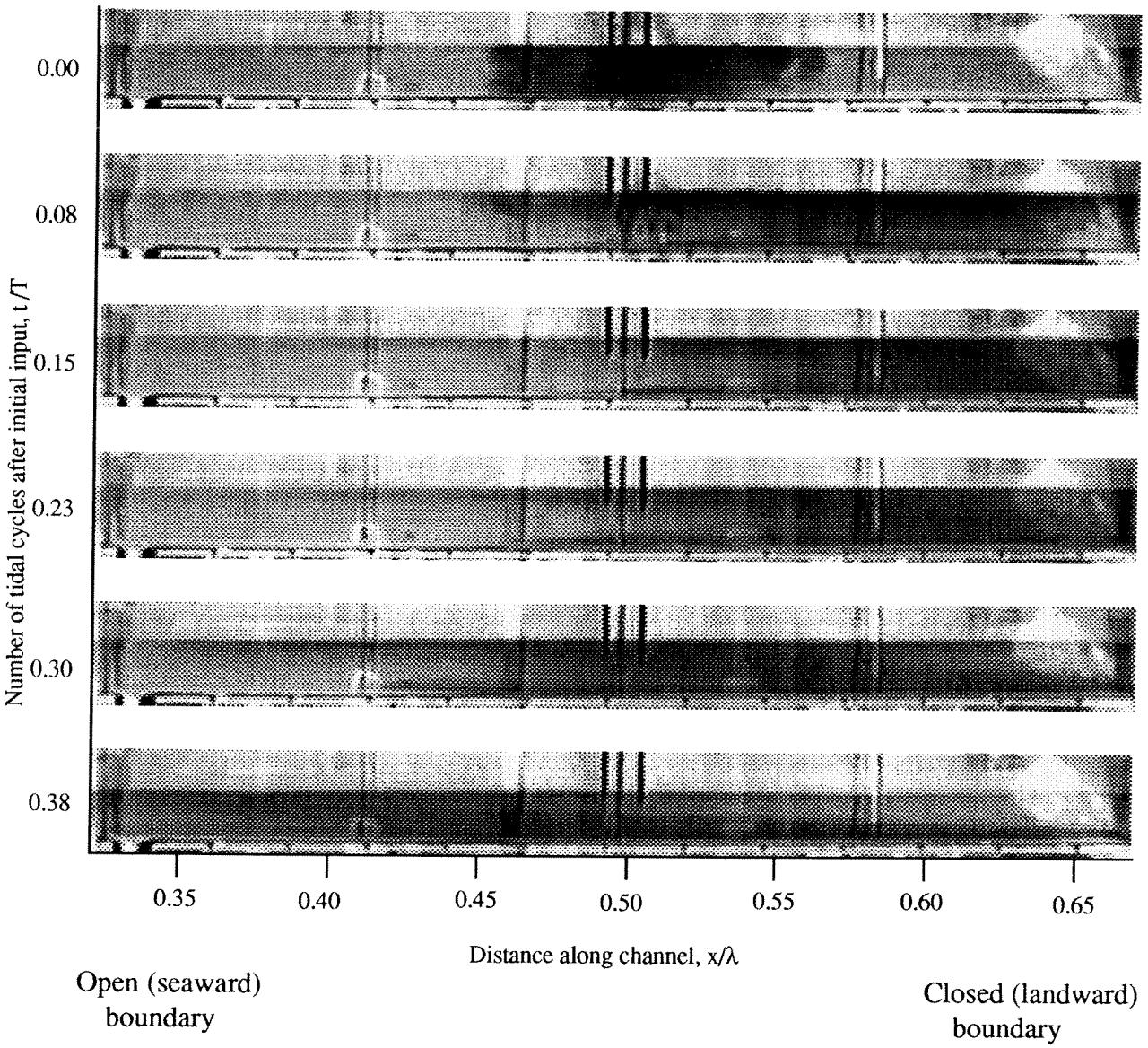

Figure 4.5 *Video images showing the movement of the pollutant cloud for the Base Case. (Input on the flood tide)*

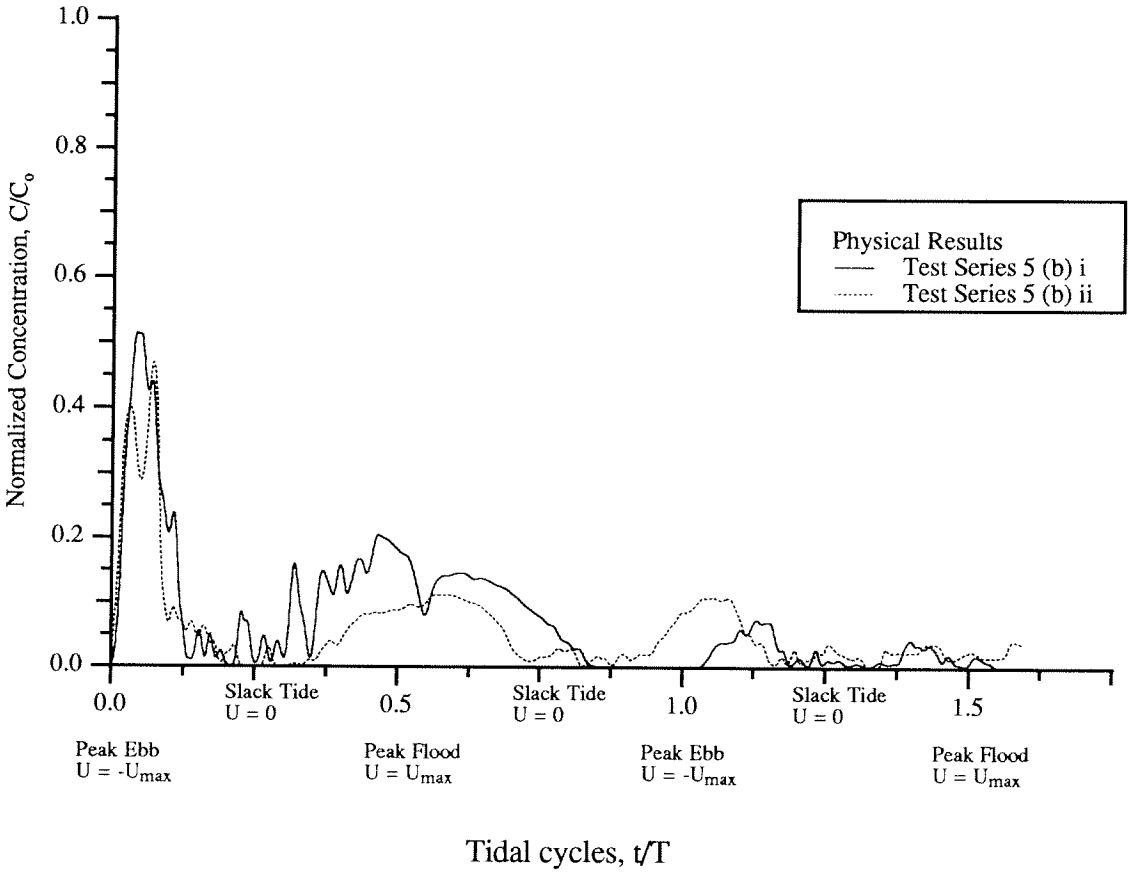

Figure 5.1 *Repeatability of effluent concentrations measurements from physical tests for the Base Case.*

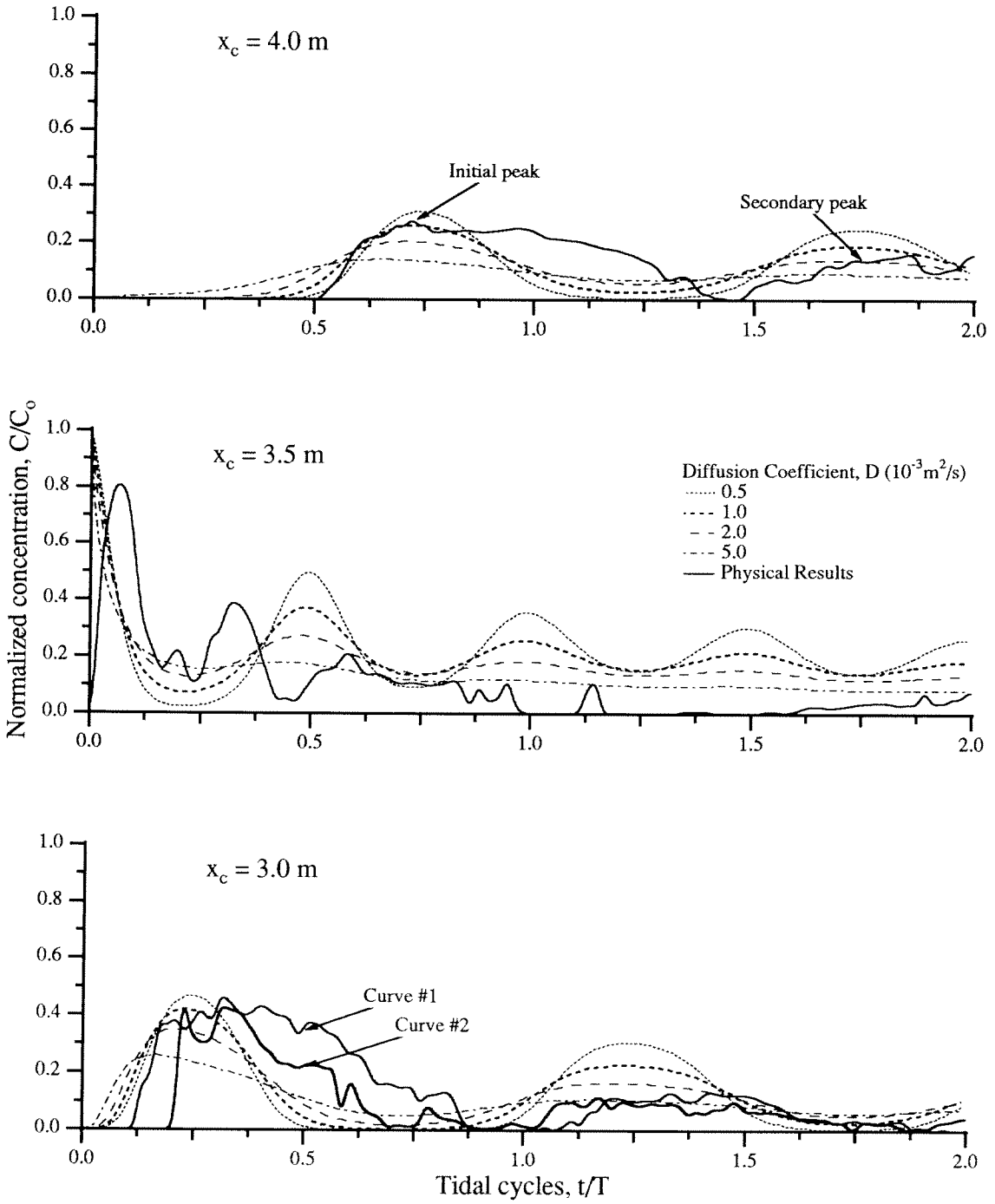

Figure 5.2 *Concentration traces at locations x_c = 3.0, 3.5, and 4.0 m comparing physical and numerical results corresponding to Test Series 2a. (Discharge at x_p = 3.5 m on the ebb tide, t_o /T = 0.0)*

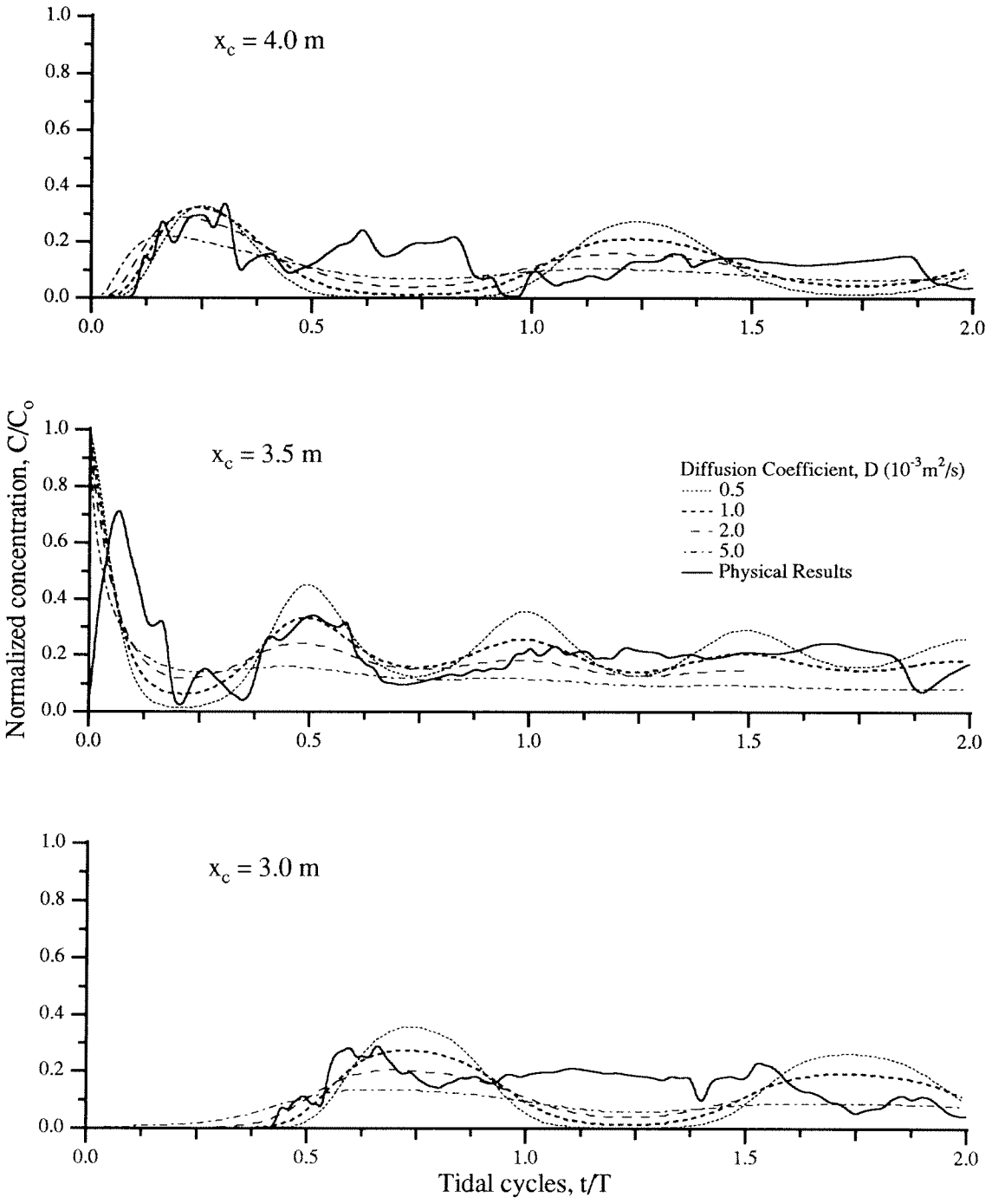

Figure 5.3 *Concentration traces at locations x_c = 3.0, 3.5, and 4.0 m comparing physical and numerical results corresponding to Test Series 2b. (Discharge at x_p = 3.5 m on the flood tide, t_o/T = 0.5)*

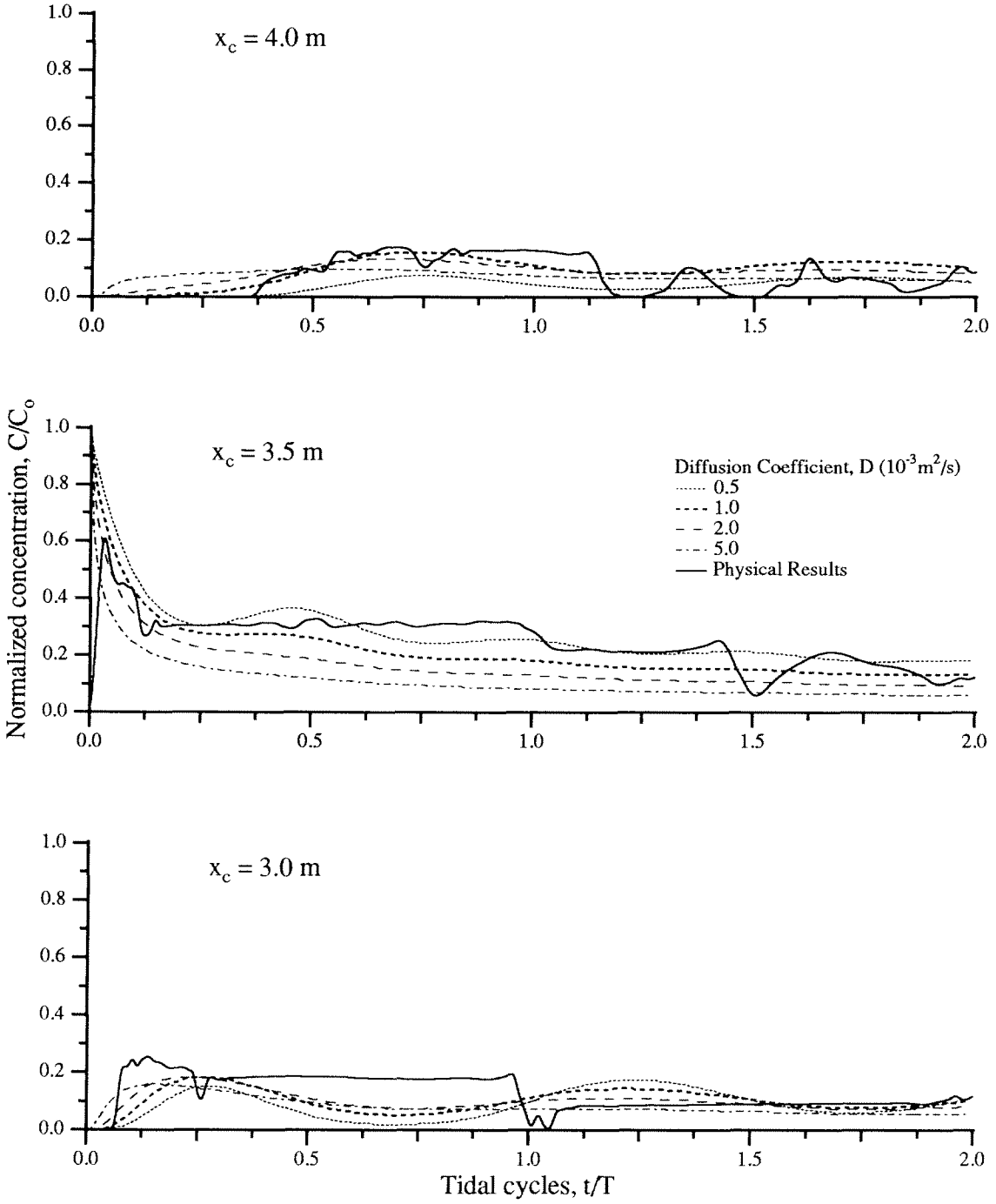

Figure 5.4 *Concentration traces at locations x_c = 3.0, 3.5, and 4.0 m comparing physical and numerical results corresponding to Test Series 3a. (Discharge at x_p = 3.5 m on the ebb tide, t_o/T = 0.0)*

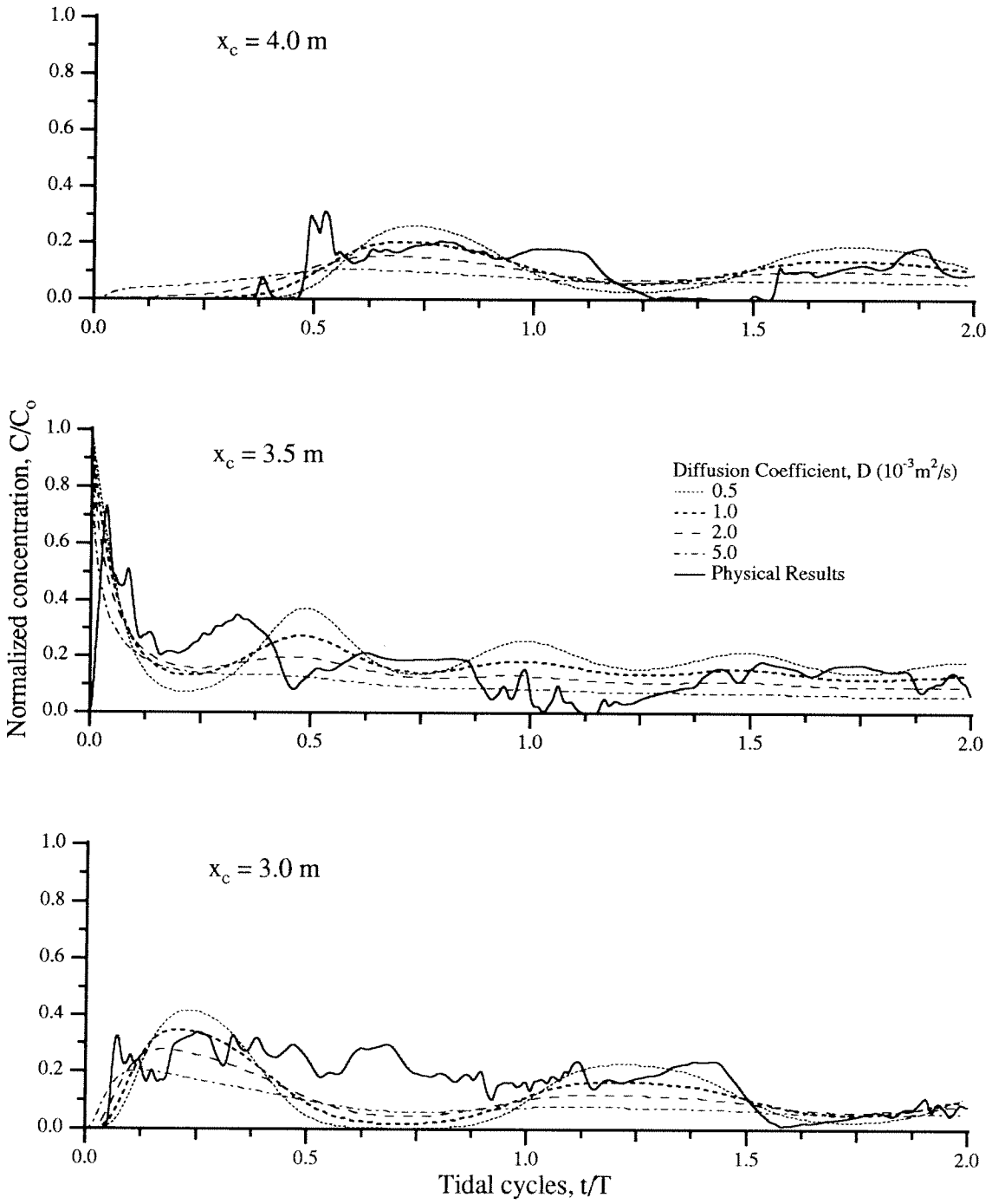

Figure 5.5 *Concentration traces at locations x_c = 3.0, 3.5, 4.0 m comparing physical and numerical results corresponding to Test Series 4a. (Discharge at x_p = 3.5 m on the ebb tide, t_o/T = 0.0)*

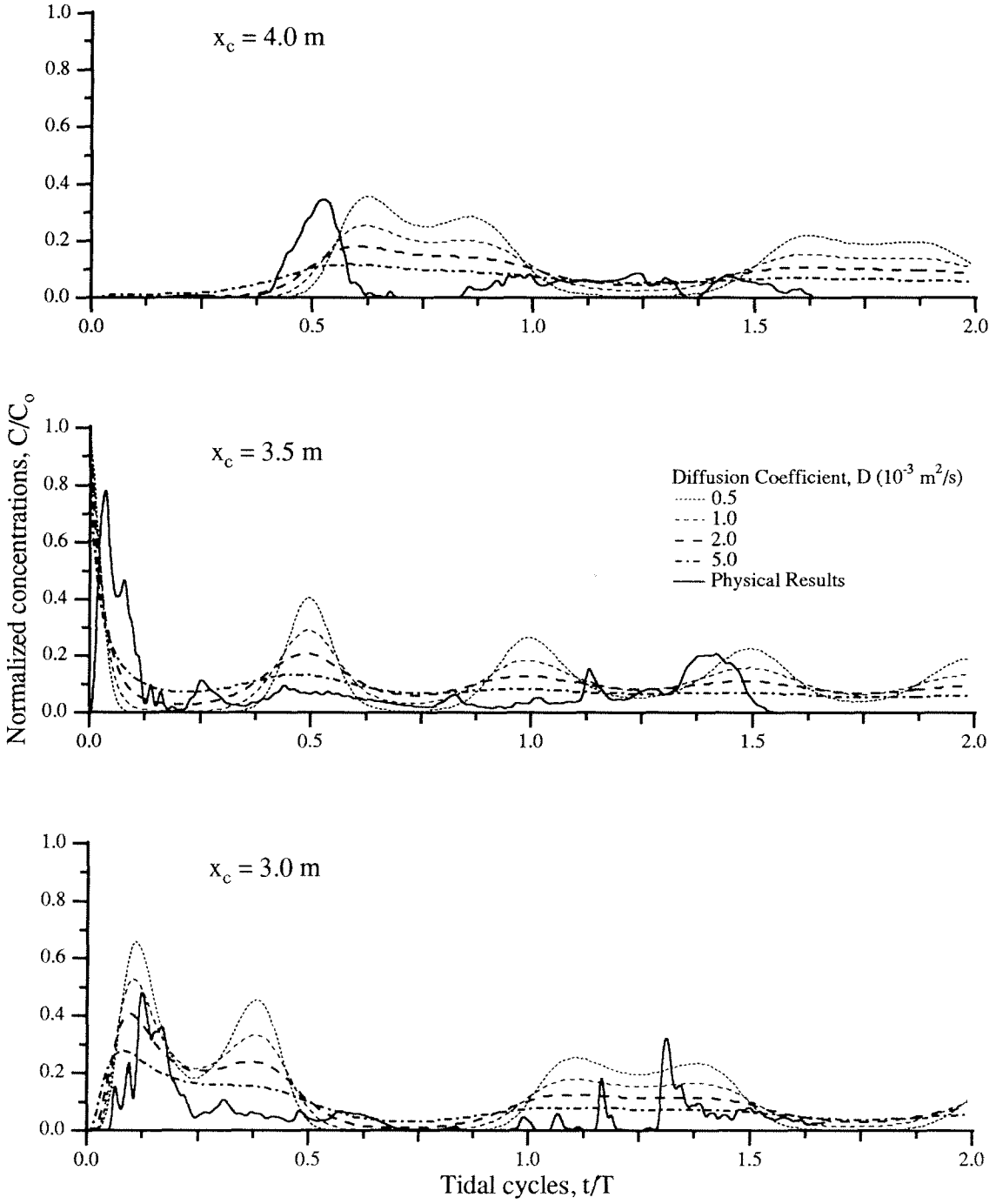

Figure 5.6 *Concentration traces at locations x_c = 3.0, 3.5, and 4.0 m comparing physical and numerical results corresponding to Test Series 5a. (Discharge at x_p = 3.5 m on the ebb tide, t_o/T = 0.0)*

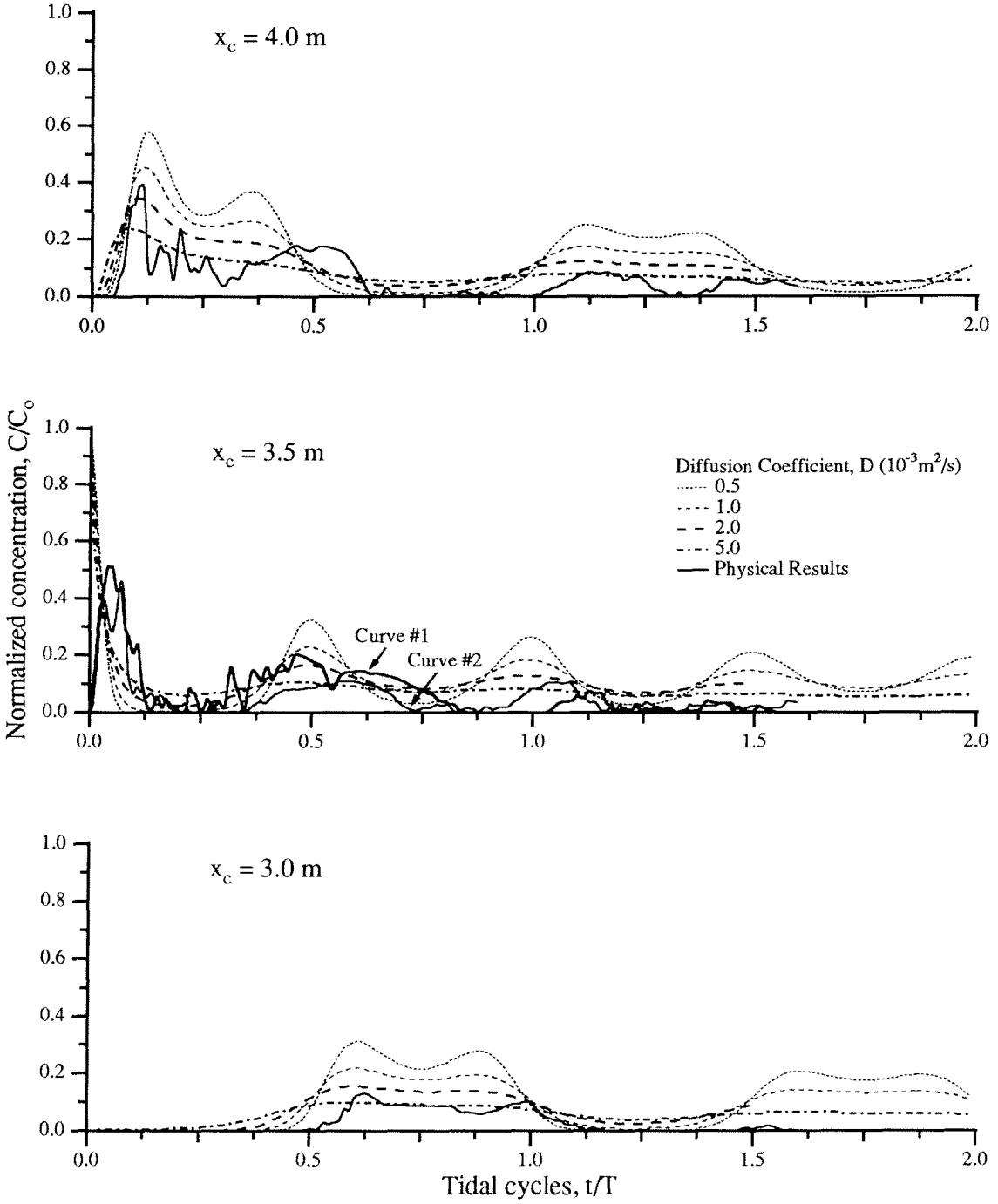

Figure 5.7 *Concentration traces at locations x_c = 3.0, 3.5, 4.0 m comparing physical and numerical results corresponding at Test Series 5b. (Discharge at x_c = 3.5 m on the flood tide, t_o/T = 0.5)*

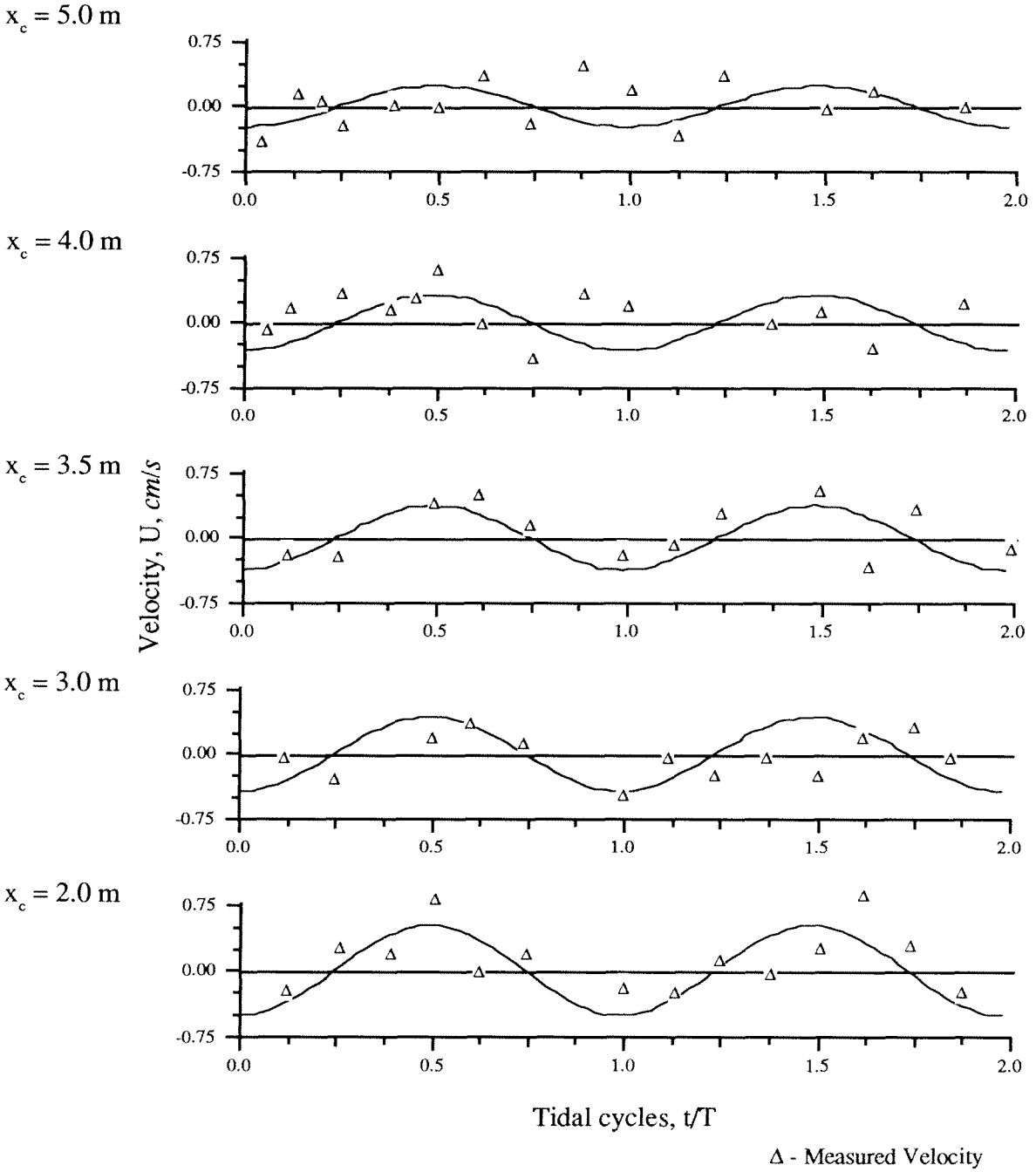

Figure 5.8 Velocity profiles comparing physical and numerical results at various locations for the Base Case.

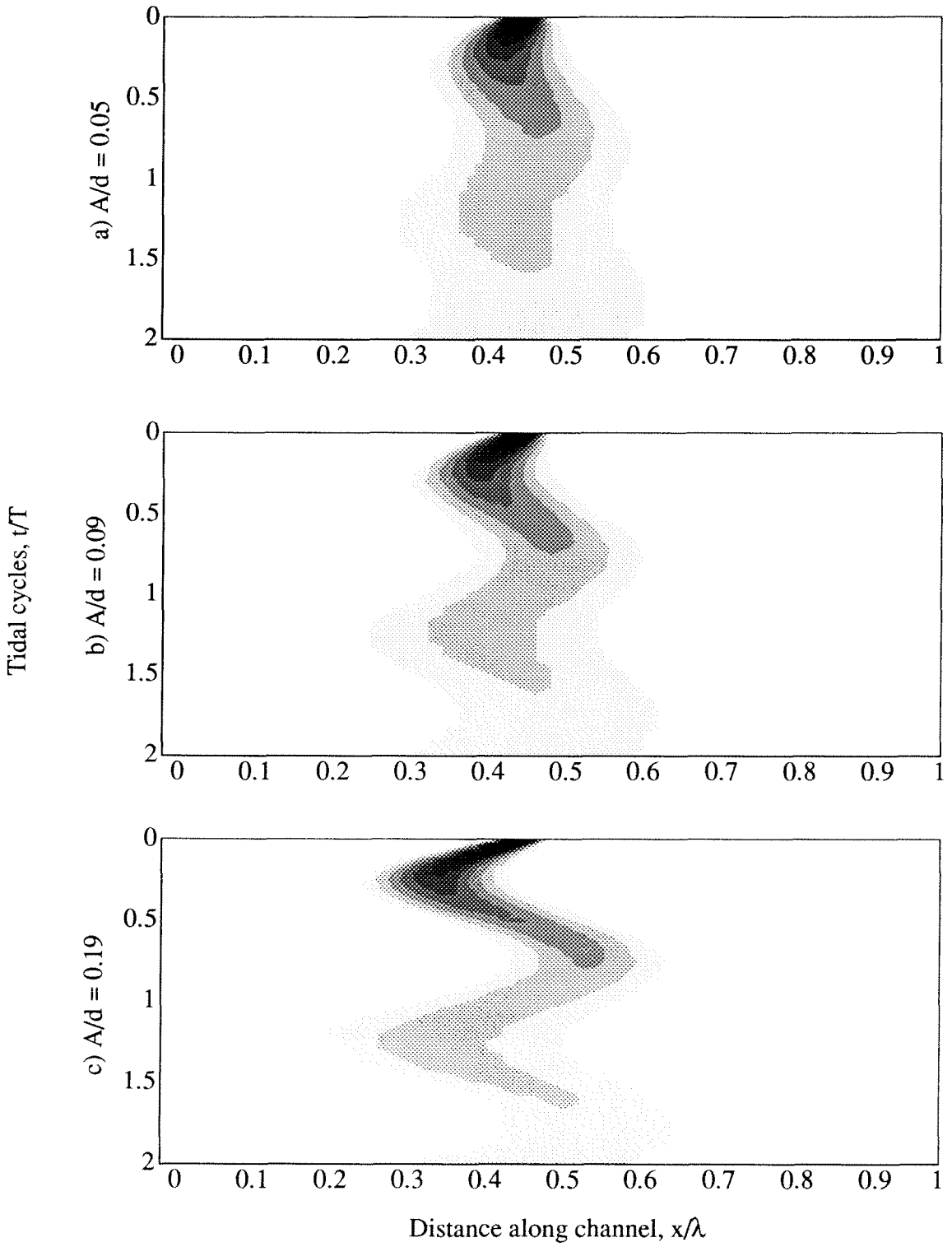

Figure 5.9 *Numerical concentration contours comparing various tidal amplitude to depth ratios, A/d = (a) 0.05, (b) 0.09, and (c) 0.19*

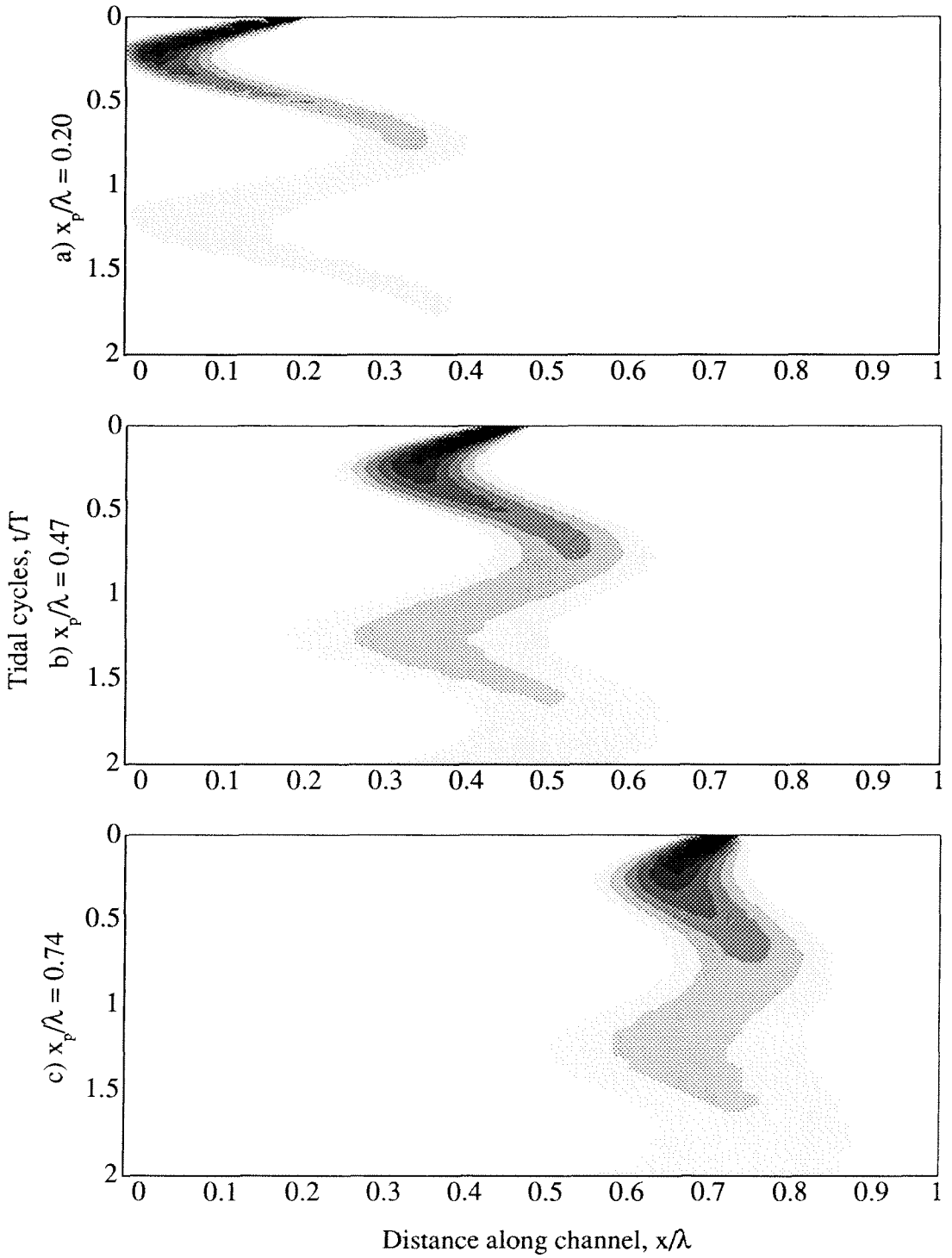

Figure 5.10 *Numerical concentration contours comparing various input positions along channel length, x_p/λ = (a) 0.20, (b) 0.47, and (c) 0.74.*

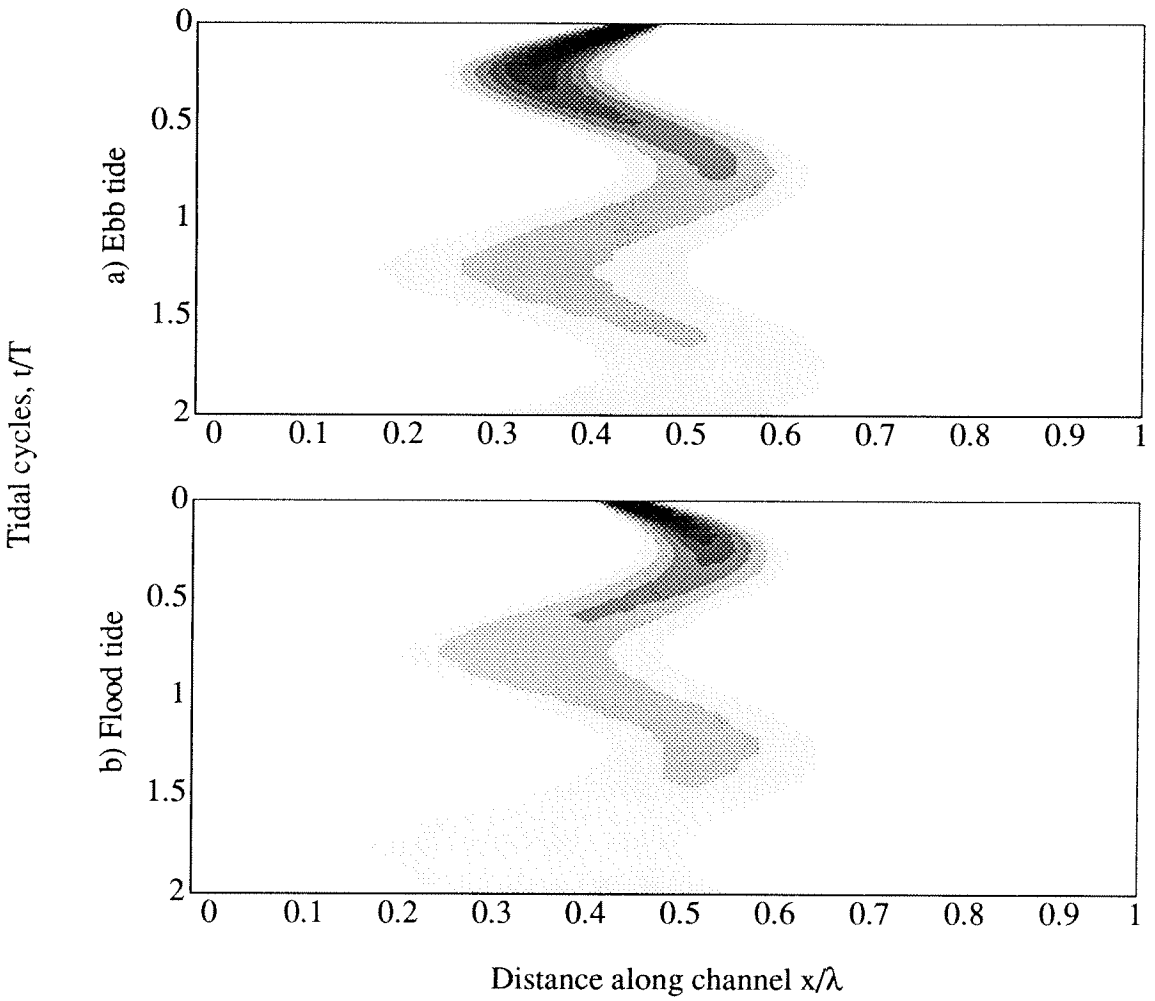

Figure 5.11 *Numerical concentration contours comparing various input times within the tidal cycle, t_p/T = input on the (a) ebb tide and (b) flood tide.*